Decoupling of net community production and particulate organic carbon dynamics in near shore surface ocean waters

Sarah Z. Rosengard[1], Robert W. Izett[1], William J. Burt[2], Nina Schuback[3], and Philippe D. Tortell[1,4]

1. Department of Earth, Ocean and Atmospheric Sciences, University of British Columbia, Vancouver, V6T 1Z4, Canada
2. College of Fisheries and Ocean Sciences, University of Alaska Fairbanks, Fairbanks, 99775, USA
3. Swiss Polar Institute, École Polytechnique Fédérale de Lausanne, Lausanne, CH-1015, Switzerland
4. Department of Botany, University of British Columbia, Vancouver, V6T 1Z4, Canada

Correspondence to: Sarah Z. Rosengard (srosengard@eoas.ubc.ca)

Abstract. We report results from two Lagrangian surveys off the Oregon coast, using continuous ship-board sensors to estimate mixed layer net community production (NCP) from variations in biological oxygen saturation ($\Delta O_2/Ar$) and optically-derived estimates of particulate organic carbon (POC). The first drifter survey, conducted in a nearshore upwelling zone during the development of a microplankton bloom, exhibited significant differences in NCP derived from $\Delta O_2/Ar$ ($NCP_{O2/Ar}$) and diurnal POC variations (NCP_{POC}), suggesting the presence of large POC losses from the mixed layer. At this site, we utilized the discrepancy between $NCP_{O2/Ar}$ and NCP_{POC}, along with additional constraints derived from surface water excess nitrous oxide (N_2O), to estimate particle export and vertical mixing fluxes. Assuming a constant background DOC production rate, export accounts for 26-69% of the daily NCP discrepancy. The second drifter survey was conducted in lower productivity offshore waters, where NCP derived from $\Delta O_2/Ar$ and POC measurements were more closely coupled, suggesting a tighter relationship between production and community respiration, and lower export rates. These results support the use of diel POC measurements to estimate NCP in lower productivity waters with limited vertical carbon export, and the potential utility of coupled O_2 and optical measurements to estimate the fate of POC in high productivity regions with significant POC export.

1 Introduction

Net community production (NCP) represents the balance between water column photosynthesis and community respiration, and sets an upper limit on the quantity of carbon produced in the mixed layer that can be transferred to the dissolved organic carbon (DOC), sinking particulate organic carbon (POC) and upper trophic levels. Accurate assessment of NCP is thus critical to understanding trophic balance and the fate of organic carbon in the surface ocean. Because traditional incubation-based approaches to quantify gross primary productivity (GPP), net primary productivity (NPP) and respiration are labor-intensive and error prone from bottle effects (Gieskes et al., 1979; Fogg and Calvario-Martinez, 1989; Marra, 2009; Quay et al., 2010), NCP remains challenging to quantify on ecologically-relevant time and space scales.

In recent years, automated *in situ* measurements of seawater optical properties have been increasingly used to estimate gross and net primary productivity (GPP and NPP, respectively) from changes in derived surface water POC concentrations (e.g., Graff et al., 2016; Burt et al.,

2018). This approach is based on the relationship between POC concentrations and the particulate fraction of the beam attenuation coefficient (c_p) (Siegel et al., 1989; Stramska and Dickey, 1992; Gardner et al., 1993; Claustre et al., 1999; Gernez et al., 2011), which can be used to resolve diurnal variations in POC. This diurnal variability results from the daytime accumulation of photosynthetically-derived organic carbon, and nighttime loss of fixed carbon through community respiration, and can be thus used to infer NCP on daily time-scales. The accuracy of this approach depends on a key assumption that variations in c_p capture most of variability in POC concentration, and it has been shown that beam attenuation is most sensitive to particles with a diameter range of 0.5–20 µm (Stramski and Kiefer 1991; Marra, 2002; Claustre et al., 2008). To date, most efforts to calculate daily NCP from c_p variability have focused on low productivity offshore regions, where particle sizes are small and particle export is limited (Claustre et al., 2008; White et al., 2017). These studies have reported good agreement between optically-derived GPP estimates and independent estimates of NPP from ^{14}C incubations (White et al., 2017), suggesting a tight coupling between primary productivity and mixed layer POC dynamics over daily time scales.

Another approach to NCP quantification is based on autonomous measurements of surface water dissolved oxygen to argon ratios (O_2/Ar). Argon normalization is used to correct for any physically-induced changes in O_2 saturation, such that the derived saturation anomaly, ΔO_2/Ar, represents the biologically-induced net O_2 production (Kaiser et al., 2005; Tortell, 2005; Cassar et al., 2009). At steady-state, and in the absence of significant lateral advection and vertical mixing, the sea-air flux of excess biologically-produced O_2 is equivalent to NCP,. With the development of automated ship-board mass spectrometers, there has been a significant increase in surface water O_2/Ar measurements, and these have been used to examine O_2/Ar variability resulting from diurnal variations of photosynthesis and respiration, and to infer NCP in a variety of oceanic ecosystems (Reuer et al., 2007; Stanley et al., 2010; Tortell et al., 2011, 2014; Hamme et al., 2012; Nicholson et al., 2015; Manning et al., 2017). Recent efforts have shown that NCP estimates from ΔO_2/Ar measurements can be corrected for vertical mixing using water column N_2O measurements as a tracer (Cassar et al. 2014; Izett et al. 2018), but most applications of this methodology still must assume that lateral advection is negligible.

Combined measurement of mixed layer POC and O_2 dynamics holds the potential to better constrain surface water carbon budgets at high spatial and temporal resolution. In net

autotrophic systems, an increase in $\Delta O_2/Ar$ reflects the accumulation of excess photosynthetic O_2 in the mixed layer, but provides no direct insight into the fate of the resulting organic carbon. In the absence of particle export, grazing or DOC production, an increase in $\Delta O_2/Ar$, corrected for air-sea exchange and vertical mixing, should be matched by a parallel increase in POC accumulation measured by optical sensors. By comparison, high POC export, grazing or DOC production would act to decouple $\Delta O_2/Ar$ from optically-derived POC measurements in the mixed layer.

Previous authors have used simultaneous O_2 and c_p measurements on moorings to describe mixed layer O_2 and POC dynamics in various marine environments (Stramska and Dickey, 1992; Kinkade et al., 1999; Dickey and Chang, 2002). However, few studies to date have compared estimates of primary productivity from simultaneous measurements on daily time scales. Briggs et al. (2018) and Alkire et al. (2012) were the first to explicitly combine concurrent measurements of O_2 and POC from *in situ* autonomous sensors to quantify mixed layer productivity during a ~2-month Lagrangian study of the 2008 North Atlantic spring bloom. Tracking daily changes in mixed layer O_2 and POC concentrations, Alkire et al. (2012) constructed a detailed budget of surface ocean organic carbon throughout the course of the bloom, using the difference between O_2-based NCP and net POC accumulation to assess the partitioning of NCP into different carbon pools (sinking particles, phytoplankton biomass, and DOC). Building on this work, Briggs et al. (2018) examined the role of respiration, particle export, and DOC production in decoupling O_2 and POC dynamics through different bloom stages, demonstrating large differences between GPP estimates derived from O_2, beam attenuation, and backscatter measurements. To our knowledge, such a detailed examination of O_2 and POC dynamics has not been reported for other marine systems.

Here, we present new results from a field study of diel variability in $\Delta O_2/Ar$ and optical properties in two contrasting near-shore regions of the Subarctic North Pacific. Using ship-board automated sensors deployed along a Lagrangian drifter track, we resolved fine-scale temporal patterns in biological oxygen production and POC concentration in a high productivity coastal upwelling zone over the continental slope and lower productivity stratified waters offshore. In these water masses with different phytoplankton community composition, we derived GPP, community respiration and NCP estimates from O_2/Ar and optically-derived POC measurements. The biogeochemical differences between both sites provided a unique opportunity to compare

NCP estimates derived from $\Delta O_2/Ar$ and POC in contrasting trophic regimes. We expected to observe significant uncoupling between $\Delta O_2/Ar$ and POC-derived NCP estimates in the higher productivity site, reflecting greater carbon export capacity and DOC production.

The results of this investigation extend findings from the 2008 North Atlantic bloom to a high productivity coastal upwelling environment, where vertical mixing fluxes significantly influence the surface water mass balance. These dynamic systems play a disproportionately important role in marine biogeochemical cycling, but they pose significant challenges for interpreting time series of ecosystem metabolism. Thus, our study further illustrates the application of a recent field approach to correcting NCP for vertical mixing (Izett et al., 2018), suggesting that this approach has significant merit in reconstructing productivity estimates from mixed layer tracers. We discuss the implications of our coupled O_2-POC measurements for understanding biological carbon cycling in coastal marine waters, and suggest additional approaches to further improve the utility of coupled $\Delta O_2/Ar$ and optically-derived organic carbon measurements for evaluating the fate of marine primary productivity across marine trophic gradients.

2 Methods

2.1 Field site and Lagrangian surveys

Field studies were conducted on board the R/V *Oceanus* in August 2017, during a transect through the Northeast Subarctic Pacific Ocean. Two Lagrangian drifters were deployed off the Oregon coast, allowing us to track diurnal patterns in phytoplankton productivity and particulate organic carbon cycling in two distinct water masses (Fig. 1). Underway temperature and salinity measurements, collected by a Seabird SBE 45 thermosalinograph, as well as satellite (Aqua MODIS) and ship-based chlorophyll-a (Chl-a) observations, were used to guide the specific location and timing of the drifter deployments. Drifter 1 was deployed on 20 August 2017 (~9:30 PDT), ~40 km from the Oregon coast (44.54° N, 124.58° W), in the vicinity of an upwelling feature detected based on low sea surface temperature, and elevated salinity and [Chl-a]. The drifter, consisting of a beacon, GPS transmitter and 5 m drogue, was recovered at ~18:30 on 23 August 2017 (44.40° N, 124.55° W) for a total deployment of 3 days and 9 hours. Upon

recovery, the drogue was missing, implying the potential for some erratic sub-surface drifting (discussed below). Drifter 2 was deployed approximately 200 km from shore (43.75° N, 126.50 °W) in a relatively warm and low salinity water mass, with low Chl-a concentrations. This second drifter was deployed at ~07:45 on 24 August 2017, and was recovered after 2 days and six hours at ~14:00 on 26 August 2017 at 43.80° N, 126.99° W. Because the *Oceanus* lacks a dynamic positioning system, the ship was not always able to perfectly track the drifter locations. To correct for these positional offsets, we discarded any observations obtained when the ship was more than 1.5 km away from the drifter location. This filtered dataset resulted in measurements every ~15 minutes during the two drifter deployments, yielding 325 and 218 quality-controlled underway observations for drifters 1 and 2, respectively.

2.2 Underway measurements

Continuous underway measurements of surface seawater optical properties were collected using Seabird ECO-BB3 and ac-s sensors, following the methods outlined in detail by Burt et al. (2018). Water was collected from the ship's seawater supply system with a nominal intake of 5 m depth. Our instrument package includes fully automated data collection, and hourly filtered blanks (0.2µm), which provide measurements of dissolved seawater optical properties used to infer particulate absorption (a_p) and beam attenuation (c_p) at 82 wavelengths between 400 and ~735 nm, and backscatter (b_{bp}) at 470 nm, 532 nm, and 650 nm. The BB-3 and ac-s measurements were binned into 1-minute intervals. Prior to binning, the absorption and beam attenuation data were first sub-sampled every 50 data acquisition cycles (~12.5 seconds) to enable faster processing time. The optical measurements were accompanied by continuous surface photosynthetically active radiation (PAR) and windspeed data obtained from a Biospherical QSR-220 PAR sensor and Gill WindObserver II ultrasonic wind sensor mounted on the ship's bow, respectively.

Chlorophyll-a (Chl-a) concentrations were derived from the particulate absorption line height at 676 nm (a_{LH}) (Roesler and Barnard, 2013). Five-minute match-ups between underway a_{LH} and discrete [Chl-a] measurements from the entire cruise transect (Sect. 2.4) were used to derive a best fit coefficient for the linear relationship between a_{LH} and [Chl-a] (r^2=0.87, n= 58, $p<0.01$). Particulate organic carbon (POC) concentrations (µg/L) were derived from particulate

beam attenuation at 660 nm ($c_{p,660}$), using the empirical model in Graff et al. (2015). Similarly, phytoplankton organic carbon (C_{ph}) concentrations were calculated, using an empirical relationship between particulate backscatter at 470 nm ($b_{bp,470}$) and [C_{ph}] in µg/L (Graff et al., 2015). We used a limited set of 5m discrete measurements (n=6) to evaluate the relationship between POC concentrations and c_p at 660nm. As shown in Fig. S1, the POC measurements were significantly correlated to c_p (r^2=0.94, $p<0.05$), with a slope and intercept of 443.2 ± 161.5 and 27.7 ± 59.3, respectively. This slope was not significantly different from that of the Graff et al. algorithm (419.8) although our y-intercept was higher. Notwithstanding the relatively small number of discrete POC samples, and some scatter around the regression line, the similarity of our POC-c_p calibration to that reported by Graff et al. (2015) suggests that our optically-derived POC estimates are relatively robust.

To obtain information on the particle size spectrum, we derived the wavelength-dependent slope of particulate backscatter by fitting the three b_{bp} coefficients (470 nm, 532 nm, 650 nm) to an exponential equation (Stramska et al., 2003; Loisel et al., 2006; Kostadinov et al., 2009). Finally, to assess interference of inorganic minerals on POC, and C_{ph} variability, we calculated the wavelength-specific bulk refractive index (η_p) from backscatter/total scatter ratios ($\frac{b_{bp}}{c_p - a_p}$) and the wavelength-dependent c_p slope, following the approach of Boss et al. (2001), Twardowski et al. (2001) and Sullivan et al. (2005).

In addition to optical measurements, the seawater biological oxygen saturation anomaly ($\Delta O_2/Ar$) was measured at ~20 second resolution using a membrane inlet mass spectrometer connected to the ship's seawater intake. The seawater ratio of dissolved O_2 and Ar was determined by diverting a continuous flow of water across a dimethylsilicone membrane interfaced with a Hiden Analytical HAL20 triple filter quadropole mass spectrometer. The O_2/Ar ratio of air-equilibrated standards ($[O_2/Ar]_{eq}$), incubated at ambient sea surface temperature, was measured every two hours. Values of $\Delta O_2/Ar$ were thus calculated as the percent deviation of seawater O_2/Ar measurements from the air-equilibrated ratio, using $\Delta O_2/Ar = 100\% * ([O2/Ar]_{meas} / [O_2/Ar]_{eq} - 1)$ (Tortell, 2005; Tortell et al., 2011).

2.3 Mixed layer depth

Over the course of both drifter deployments, we conducted regular hydrographic casts (every six to ten hours) to examine depth profiles of seawater hydrography and biogeochemical variables. Temperature, salinity, dissolved O_2 concentrations and Chl-a fluorescence profile data from the CTD casts were measured by a Seabird-SBE 38 temperature sensor, Seabird-SBE 4 conductivity sensor, SBE 43 dissolved O_2 sensor, and a Seabird ECO fluorometer, respectively, and binned into 1 m intervals. Due to recent upwelling, vertical profiles at the drifter 1 site showed relatively weak density stratification. For this reason, we estimated mixed layer depths (z_{mld}) based on visible inflection points in the dissolved [O_2], fluorescence and density profiles, assuming that dissolved O_2 concentrations and fluorescence are relatively uniform in the mixed layer. Within a single CTD cast, mixed layer depths varied by up to 28% across all three profile measurements. The [Chl-a] fluorescence profiles had most well-defined inflection points, and we thus used these data to estimate z_{mld} at all casts. Excluding fluorescence profiles from the first day (Sect. 3.1), and two casts at 6am and midnight on second and third 24-hour intervals, respectively, which displayed an anomalously shallow z_{mld} (< 10 m) and relatively noisy density profiles, an average z_{mld} value (19 ± 2 m) was applied to all subsequent analyses.

In comparison to the drifter 1 site, CTD cast profiles during drifter deployment 2 showed larger density gradients. We thus computed z_{mld} using a density difference criterion of 0.25 kg/m^3 (Thomson et al., 2003; de Boyer Montégut et al., 2004) from median values within the upper-most 4–6 m of the profile. We found that this critical density criterion was necessary to capture the depth of inflection. In all CTD casts except one, density difference-based z_{mld} values were within 5 meters of the values derived from the inflection points on density profiles. An average z_{mld} value estimated from the density-difference approach (22 ± 5 m) was applied to all subsequent analyses.

2.4 Discrete samples

Concentrations of phosphate ([PO_4^{3-}]), dissolved silica ([SiO_2]), and nitrate and nitrite ([$NO_3^- + NO_2^-$], were measured in seawater samples collected from daily Niskin bottle casts. Following collection, nutrient samples were filtered through 0.2 µm pore polycarbonate membranes and immediately frozen at -80°C on board the ship. These samples were stored at -

20°C until subsequent colorimetric laboratory analyses (Murphy and Riley, 1962; Riley, 1977) with a Lachat QuikChem 8500 Series 2 Flow Injection Analysis System.

Concentrations of dissolved oxygen (O_2) and nitrous oxide (N_2O) were measured in discrete samples collected in Niskin bottles during both drifter deployments (Fig. S1), following methods outlined in (Capelle et al., 2015). These N_2O measurements were used to correct NCP estimates for vertical mixing (see Sect. 2.6), following the approach described by Cassar et al. (2014) and Izett et al. (2018). Only profiles collected during casts at 12:00 (PDT) August 21 and 23 were applied to the NCP mixing correction during drifter deployment 1. The other two profiles were not utilized because temperature and salinity data indicated potential intrusion of an external water mass with a different water column [O_2] and [N_2O] signature.

Surface (~5 m) discrete seawater samples were collected either from Niskin bottles or from the ship's surface seawater intake system for HPLC analysis of Chl-a concentrations and other phytoplankton pigments. Single or duplicate samples were filtered onto 25 mm GF/F filters, flash-frozen in liquid nitrogen, and stored at -80°C until analysis, following the methodology described in (Schuback et al., 2016). Additional samples were collected from the seawater intake for size-fractionated Chl-a analysis (Zeng et al., 2018). These samples were filtered through stacked 47 mm filters (0.2 µm, 2 µm and 20 µm pore size) separated by a mesh spacer. Filtered samples were extracted in 5 mL of 90% acetone at 4°C until analysis within 24–48 hours using a Turner Trilogy Fluorometer on board the ship.

Discrete samples for POC analysis were collected at two depths from several CTD casts. Surface samples were collected at both drifter sites from 5 m depth, while deeper samples were collected at near the base of the euphotic zone (~1% PAR), corresponding to 40–60 m at drifter site 1, and 100–120 m at drifter site 2. POC samples (~1–4 L) were filtered through a pre-combusted (450 °C) Whatman GF/F filter (nominal pore size ~ 0.7 µm), and stored at -80°C until laboratory analysis. Prior to analysis, samples were thawed and dried at 50°C overnight, fumigated with concentrated hydrochloric acid for 48 hours, and dried again at 50°C overnight. POC concentrations in samples (and blank combusted filtered treated as described above) were quantified using an *Elementar* vario MICRO cube CHNS analyzer. Blank-corrected discrete POC concentrations were used to validate application of the [POC] model in Graff et al. (2015) to our underway c_p data (Sect. 2.2; Fig. S2).

2.5 Net Primary Productivity

Daily-integrated net primary productivity (NPP) was calculated in two ways. First, carbon uptake was determined from 24-hour ^{14}C-incubations with 5 m triplicate seawater samples collected from early morning CTD casts. Measurements were made on two different mornings during drifter deployment 1 and on one morning during drifter deployment 2. The measurements were conducted following the protocol outlined in Hoppe et al. (2017). Depth-integrated NPP was calculated by multiplying the derived 24-hour volumetric carbon fixation rate by the average mixed layer depth for the respective drifter period.

Second, daily-integrated net primary productivity was also estimated as a product of [C_{ph}] values derived from b_{bp}, and phytoplankton growth rates according to the carbon-based productivity model (CbPM) (Behrenfeld et al., 2005; Westberry et al., 2008; Graff et al., 2016; Burt et al., 2018). In these calculations, daily-averaged [C_{ph}], [Chl-a]/[C_{ph}], and mixed layer irradiance (E_g) calculated from the MODIS-derived surface PAR matched to drifter location were used to calculate growth rates and NPP every 24 hours. Chlorophyll-a concentrations were derived from absorption line height (Sect. 2.2), [C_{ph}] values from b_{bp}, and light extinction coefficients (K_d) used to calculate E_g from [Chl-a] (Morel et al., 2007). An average mixed layer depth for each drifter period was applied to estimate mixed layer NPP (Sect. 2.3).

2.6 Quantification of diurnal cycles and NCP

We quantified net community production (NCP) based on the analysis of diurnal variations in $\Delta O_2/Ar$ ($NCP_{O2/Ar}$) and POC (NCP_{POC}) based on linear regressions of measurements against time over subsequent day and night intervals. This approach, using all data points, minimizes uncertainty in the derived rates of change relative to an approach based on a two-point difference in ΔO_2 or ΔPOC over 24-hours. In all calculations described below, daily-integrated NCP values were taken as the sum of daytime (D) and nighttime (N) values. Daytime was defined as the period during which PAR levels exceeded 20 µmol quanta $m^{-2}s^{-1}$. The average length of the day-time period, t_D, was 13.6 ± 0.14 hours over the two drifter deployments. Daily NCP values were integrated through the mixed layer using the average z_{mld} for each drifter period, as described in Sect. 2.3.

Net community production can be calculated over shorter time scales (e.g., Tortell et al., 2014), but this approach was not feasible with our data set, given that the average measurement interval was ~15 minutes after removing values where the ship was not sufficiently close to the drifter (Sect. 2.1). Nonetheless, we found that calculation of NCP over 3-hour increments followed by integration into 24-hour periods were generally consistent with NCP calculated using daily-integrated terms (Table 1). The differences in shorter term estimates vs. daily-integrated values are primarily due to the effect of lower signal to noise in $\Delta O_2/Ar$, $[O_2]_{bio}$ and [POC] variations within these shorter time intervals.

2.6.1 O_2/Ar-derived NCP

Quantification of NCP from diurnal cycles in $\Delta O_2/Ar$ requires corrections for gas exchange and, potentially, vertical mixing fluxes. For these calculations, we first computed the rate of change in $\Delta O_2/Ar$ (dO_{2Bio}/dt) using linear regression analysis within successive daytime or nighttime intervals. We then derived estimates for the air-sea gas exchange (J_{ex}) and vertical mixing fluxes (F_{mix}) over the respective day or night interval to isolate the NCP contribution to observed $\Delta O_2/Ar$ changes (Izett et al., 2018; Tortell et al., 2014). Net O_2 production rates were converted into carbon units using a photosynthetic quotient (PQ) for new production of 1.4 for drifter period 1 calculations and a PQ for regenerated production of 1.1 for drifter period 2 (Laws, 1991).

$$NCP_{O2/Ar} = \frac{t_d NCP_D + t_N NCP_N}{PQ} \quad (1)$$

$$NCP_{D\ or\ N} = z_{mld} \frac{dO_{2bio}}{dt} + J_{ex} + F_{mix} \quad (2)$$

$$O_{2bio} = \frac{\Delta O_2}{Ar} \frac{1}{100\%} O_{2eq} \quad (3)$$

$$J_{ex} = k_{o2} O_{2bio} \quad (4)$$

$$F_{mix\,(\frac{O_2}{Ar})} = k_{mix}\frac{dO_{2bio}}{dz} \quad (5)$$

$$k_{mix} = k_{N2O}N2O_{bio}(\frac{dN2O_{bio}}{dz})^{-1} \quad (6)$$

$$N_2O_{bio} = N2O_{meas} - N2O_{eq} - N2O_{thermal} \quad (7)$$

Equilibrium concentrations of O_2 and N_2O ($[O_2]_{eq}$ and $[N_2O]_{eq}$) were calculated using the salinity and temperature-dependent equations of Garcia and Gordon (1992) and Weiss and Price (1980), respectively, and sea surface temperature and salinity from the ship's thermosalinograph. Estimates of surface excess N_2O saturation, $[N_2O]_{bio}$, included a heat flux correction to account for solubility changes (Keeling and Shertz, 1992; Jin et al., 2007; Izett et al., 2018). Non-weighted piston velocities (k_{O2} and k_{N2O}) were calculated using the diffusive air sea gas flux and Schmidt number parameterizations of Wanninkhof (2014) and Raymond et al. (2012), and ship-based wind speed data 10 m above the sea surface. Daytime and nighttime estimates for the gas exchange term, J_{ex}, were calculated using day/night average $[O_2]_{eq}$, $\Delta O_2/Ar$, and k_{O2} values. Daytime and nighttime F_{mix} was calculated using $[N_2O]_{bio}$ values averaged over the entire drifter deployment, daytime/nighttime average k_{N2O} values, and a vertical gradient term derived from all of the O_2 and N_2O profile data for the cruise (Sect. 2.4). At drifter site 2, vertical mixing was considered negligible in the absence of N_2O super-saturation in surface waters (Fig. S1) (Izett et al., 2018). Further, at drifter site 1, denitrification was considered a negligible source of N_2O within the upper 100 m of the water column because measured O_2 concentrations were consistently greater than the threshold value of ~50 mmol m^{-3} (e.g., Hopkinson and Barbeau, 2007). Likewise, we assumed no lateral advection of N_2O into drifter site 1, as there were little differences in the mixing ratio $[O_2]_{bio}/[N_2O]_{bio}$ across profile measurements (Fig. S1).

2.6.2 Optically-derived NCP

We used the approach of (Claustre et al., 2008; White et al., 2017) to calculate daily-integrated NCP from daytime and nighttime changes in POC (dPOC/dt), calculated from linear regressions of POC concentrations against time through day and night intervals.

$$NCP_{POC} = z_{mld}\left[t_D\left(\frac{dPOC}{dt}\right)_D + t_N\left(\frac{dPOC}{dt}\right)_N\right] + F_{mix\,(POC)} \quad (8)$$

In certain ocean environments, NCP_{POC}, as defined above, will not equate to $NCP_{O2/Ar}$ as a result of additional POC sinks, including export, grazing and DOC production. Under these conditions, NCP_{POC} more accurately reflects net POC accumulation. Nonetheless, for consistency with previous studies, we use the term NCP_{POC} to describe the quantity computed in Eq. 8.

The presence of significant upwelling at drifter site 1 (Fig. 1) provides additional complexity in the estimate of NCP from derived-POC measurements. In particular, entrainment of particle-poor seawater from below the mixed layer into the surface could dilute the c_p signal used to derive POC concentrations (Stramska and Dickey, 1994). To address this, we applied the vertical mixing term, k_{mix}, derived from Eq. (6) to estimate the average daily dilution effect on mixed layer POC concentrations through drifter period 1:

$$F_{mix\,(POC)} = k_{mix}\frac{dPOC}{dz} \quad (9)$$

The term d[POC]/dz represents the vertical gradient in [POC], derived from average POC concentrations measured in CTD samples at 5 m and near the base of the euphotic zone, below the mixed layer (40–60 m) (Sect. 2.4). The dz term was calculated as the difference between the average mixed layer depth and the average shallowest depth of minimum particle concentrations, based on beam transmission profiles obtained from the CTD rosette. The uncertainty associated with this gradient calculation is addressed in the discussion section. At drifter site 2, $F_{mix,POC}$ was assumed to be negligible since the derived vertical mixing term was close to zero.

In total, three $NCP_{O2/Ar}$ and NCP_{POC} values were calculated during the drifter 1 deployment, from the three pairs of consecutive day and night intervals, starting with the first night interval and ending with the last day interval. We excluded the first day-time interval from our calculations, due to the erratic salinity values observed during the first day of this drifter deployment (Sect. 3.1; Fig. S2). Because the drifter period was terminated prior to sunset, the last day interval was 1.6 hours shorter than the average daytime duration. For the second drifter deployment, two $NCP_{O2/Ar}$ and NCP_{POC} values were calculated from consecutive day and night

intervals, starting with the first daytime interval and ending with the last nighttime interval. The initiation of the drifter period occurred after sunrise, so the first day interval was 1.1 hours shorter than the average daytime duration.

2.7 Error analysis

Errors for all estimates of net primary productivity (CbPM-NPP, ^{14}C-NPP) and net community production ($NCP_{O2/Ar}$, NCP_{POC}) were propagated from uncertainties associated with all variables used for the computations, including the standard deviations of all time-averaged variables. The uncertainty in z_{mld}, or the standard deviation of mixed layer depths across individual CTD casts, was 2 m for drifter site 1 and 5 m for drifter site 2 (Sect. 2.3). Small uncertainties in t_D and t_N were calculated as the standard deviations of all day or night lengths measured during both drifter periods (0.14 and 0.10 hours, respectively). Mean relative errors of [Chl-a] and [C_{ph}] from Burt et al. (2018), and mean relative standard deviations in MODIS-derived daily surface PAR values were propagated to calculate the error in CbPM-NPP. The standard deviations of triplicate 24-hour ^{14}C uptake incubations were propagated to calculate the error in ^{14}C-NPP estimates. The uncertainties in ^{14}C-NPP values are likely underestimated, as they do not account for bottle effects, as discussed in Sect. 4.3.

For calculating error in NCP, uncertainties in dO_{2bio}/dt and dPOC/dt were derived from the confidence interval of the best-fit slope of linear regression of each variable against time. Standard deviations of averaged $\Delta O_2/Ar$, k_{O2}, $d[O_2]_{bio}/d[N_2O]_{bio}$ and $d[N_2O]_{bio}/dz$ values, and the mean relative errors of k_{N2O}, $[N_2O]_{meas}$, $[N_2O]_{Eq}$, and $[N_2O]_{thermal}$ reported in Izett et al. (2018), were propagated into errors for $NCP_{O2/Ar}$ and NCP_{POC}. Finally, to account for uncertainty in the photosynthetic quotient (PQ), we applied a PQ variability of 0.1 to $NCP_{O2/Ar}$ calculations, following Laws (1991).

3 Results

3.1 Water mass properties

Ship-board underway measurements revealed clear differences in hydrographic and biogeochemical characteristics between the water masses sampled by the two drifters. Surface water properties at drifter site 1 reflected the presence of a recently upwelled water mass that was relatively cold (11.8 ± 0.4 °C), saline (32.6 ± 0.04 g/kg), and nutrient-rich (Figs. 1, S3, S4). The Pacific Fisheries Environmental Laboratory's coastal upwelling index at 45°N, 125°W was positive throughout drifter period 1. In contrast, the water mass tracked by the second drifter deployment was warmer (17.5 ± 0.1°C) and fresher (31.8 ± 0.05 g/kg), with lower average mixed layer nutrient concentrations.

Examination of surface water hydrographic properties during the two drifter deployments suggest that both drifters tracked a relatively homogenous water mass, excluding a period of salinity variability during the first day of drifter deployment 1, and several transient temperature and salinity excursions after the second night of this deployment (grey patches in Fig. S3). These features indicate potential intrusion of an external water mass, possibly a result of loss of the drifter drogue (Sect. 2.1). Observations during these periods were thus removed from the data set prior to analysis. Outside of these intervals, variability in salinity (drifter 1: 32.5–32.7 g/kg; drifter 2: 31.8–31.9 g/kg) was small during both drifter deployments. Variability in sea surface temperature was also limited (drifter 1: 11.2–13.0 °C, drifter 2: 17.3–17.7 °C), and largely reflected a diurnal variation of warming and cooling, which was particularly evident for drifter period 2.

Temporal differences in CTD cast profiles point to some variation in mixed layer depth (z_{mld}) during both drifter deployments. In general, there were no multi-day trends in z_{mld} through both periods, suggesting that transient shifts in water column turbulence likely contributed to changes in the shape of temperature, salinity, dissolved oxygen and fluorescence profiles. Average z_{mld} values, calculated over each drifter period, had relatively low relative standard deviations (<25%) and were applied to all subsequent calculations (Sect. 2.3). A sensitivity analysis, not shown, indicated that the choice of mixed layer depth using different criteria (i.e., fluorescence profiles, density profiles and the density difference criterion) and different time scales of integration (i.e., daytime/nighttime, 24 hour, and multi-day) did not significantly impact the results discussed below.

Average mixed layer nutrient concentrations fluctuated during both drifter deployments, but did not exhibit regular diurnal cycles (Fig. S4). At drifter site 1, concentrations ranged from

0.74 to 0.85 µM phosphate, 7.8 to 9.0 µM nitrate and nitrite, and 9.2 to 11.1 µM dissolved silica, excluding day 1 of the drifter deployment and anomalously high concentrations measured during a noisy CTD cast at midnight on the last day of the deployment. Excluding these outliers, a significant ($p<0.05$) linear regression of each nutrient concentration against time revealed that phosphate concentrations decreased by ~0.07 µM, [NO_3^- + NO_2^-] decreased by 0.9 µM, and [SiO_2] decreased by 1.2 µM over the three-day drifter period. Nutrient concentrations varied less at site 2, from 0.08–0.10 µM [PO_4^{3-}], 0.29–0.61 µM [NO_3^- + NO_2^-], and 1.2–1.7 [SiO_2]. While [PO_4^{3-}] and [SiO_2] increased significantly ($p<0.05$) by 0.015 µM and 0.48 µM, respectively, the change was small compared to the shift observed during drifter period 1.

3.2 Biogeochemical comparisons between drifter sites

Elevated nutrient concentrations at the drifter 1 site supported high productivity and the accumulation of phytoplankton biomass, as indicated by elevated chlorophyll-a ([Chl-a]= 0.66–1.5 µg/L), phytoplankton carbon ([C_{ph}]= 83–115 µg/L) and particulate organic carbon concentrations ([POC]= 130–261 µg/L) (Figs. 2a–c). We observed [C_{ph}]/[Chl-a] ratios ranging from 68–143 g/g, with a median value of 85 g/g (Fig. 2f). Using the carbon-based production model (CbPM; Sect. 2.5) and daily-averaged mixed layer PAR derived from satellite values matched to drifter location (within 5 km), these [C_{ph}]/[Chl-a] ratios translate into phytoplankton growth rates ranging from 0.75–0.94 d^{-1}. At the second drifter site, phytoplankton productivity and biomass were significantly lower in the nutrient-poor waters ([Chl-a]= 0.06–0.21 µg/L, [C_{ph}]= 11–17 µg/L, and [POC]= 25–38 µg/L). Ratios of [C_{ph}] to [Chl-a] at site 2 were significantly higher ($p<0.05$) than those observed at site 1, ranging from 69 g/g to 203 g/g, with a median value of 108 g/g. The higher ratios may reflect reduced cellular [Chl-a] associated with greater nutrient limitation, higher daily-integrated PAR, and proportionally more picoplankton than microplankton at drifter site 2 (Westberry et al., 2008; Hirata et al., 2011; Graff et al., 2016; Burt et al., 2018). Median PAR levels were higher and less variable at site 2, in part contributing to lower variability in CbPM-based growth rates, which ranged from 0.81 to 0.85 d^{-1}.

Several lines of evidence suggest that the phytoplankton assemblage at drifter site 1 was enriched in large-celled phytoplankton, as compared to drifter site 2. The wavelength-dependent slope of particulate backscatter (b_{bp}) was lower at site 1 (range: 1.4 to 1.6, median: 1.5) than at

site 2 (1.9–2.3, median = 2.1) (Fig. 2d), suggesting proportionally larger particle sizes (Stramska et al., 2003; Kostadinov et al., 2009). This observation is supported by size-fractionated Chl-a measurements. During the drifter 1 deployment, the >20 μm size fraction (Sect. 2.4), increased from 21 % to 46 % of the total Chl-a pool, indicating the enrichment of large phytoplankton in the assemblage. Indeed, pigment-based estimates of phytoplankton taxonomic composition and size class (Hirata et al., 2011; Zeng et al., 2018) suggested that relative diatom and microplankton abundances exceeded 50 % on the final sampling time point. By comparison, size-fractionated [Chl-a] and HPLC analyses from drifter 2 indicated a lower proportion of large-celled phytoplankton, with 9–15 % of total Chl in the >20 μm size fraction, and diatoms and micro-plankton comprising 19–29 % of the phytoplankton assemblage. The proportion of picoplankton increased through time at drifter site 2 from 31–50 % of total [Chl-a], alongside slight increase in b_{bp} slope, indicating accumulation of smaller particle sizes (Fig. S3d). Finally, median bulk refractive index values across three wavelengths (470 nm, 532 nm, 650 nm) were higher at site 1 (1.08–1.11) than at site 2 (1.02–1.04) (Fig. S3e), which is consistent with a greater proportion of diatom-derived amorphous silica in the particle pool (Lide, 1997; Twardowski et al., 2001).

3.3 Diurnal variability and net community production

As shown in Fig. 3a, clear diurnal cycles in biological oxygen saturation ($\Delta O_2/Ar$) were observed during both drifter deployments. Slopes of linear regressions of $\Delta O_2/Ar$ against time were generally positive in the daytime, and negative at night (Fig. S5a). During drifter deployment 1, this diurnal cycle was superimposed on a longer-term increase in biological O_2 saturation as under-saturated values returned toward atmospheric equilibrium. At least part of this increase is attributable to gas exchange, which would act to erase O_2 under-saturation in the mixed layer caused by recent upwelling. However, calculation of the sea-air O_2 flux shows that, except for the first 24 hour period, only a small amount of the daily increase in $\Delta O_2/Ar$ can be explained by gas exchange (J_{ex} < 10 mmol O_2 m^{-2} d^{-1}). We thus attribute the temporal $\Delta O_2/Ar$ change to a primarily biological source. During drifter deployment 1, net community production calculated from diurnal $\Delta O_2/Ar$ variations, corrected for gas exchange and vertical mixing

($NCP_{O2/Ar}$), was 145 mmol C-m^{-2} d^{-1} during the first 24 hours, decreasing to 100 mmol C-m^{-2} d^{-1} during the second day, and returning to 165 mmol C-$m^{-2}d^{-1}$ on the last day (Fig. 4).

Examination of the diel variability in POC and Chl-a revealed significant differences in the behavior of these variables as compared to $\Delta O_2/Ar$ (Fig. 3b, c). Whereas $\Delta O_2/Ar$ increased during the first drifter deployment, [POC] and [Chl-a] values decreased. Vertical mixing ($F_{mix,POC}$), accounted for 36 mmol m^{-2} d^{-1} of these daily changes in [POC]. Daily-integrated net community production (NCP) calculated using diurnal variations in [POC] was positive (66 mmol C-m^{-2} d^{-1}) during the first 24-hour period, negative (-29 mmol C m^{-2} d^{-1}) during the second day, and close to zero (-9 mmol C m^{-2} d^{-1}) during the third day.

Daily averaged net primary productivity (NPP), derived from the CbPM model (Sect. 2.5), declined from 147 mmol C m^{-2} d^{-1} on day 1 of drifter deployment 1 to 112 mmol C m^{-2} d^{-1} on day 3 (Table 1), reflecting the trend in Chl-a concentrations used to derive NPP (Fig. 3c). The CbPM-derived NPP estimate was similar to that obtained in ^{14}C incubations (150 ± 18 mmol C-$m^{-2}d^{-1}$) within the first 24 hours of drifter deployment 1. However, ^{14}C-based NPP estimates on the third day of the deployment (49 ± 8 mmol C-$m^{-2}d^{-1}$) were about two-fold lower than those obtained from CbPM calculations.

NCP dynamics at drifter site 2 differed significantly from those observed at site 1. Daily-integrated NCP was lower at drifter site 2, consistent with the lower observed phytoplankton biomass and nutrient concentrations. Compared to the drifter site 1, diel variability in $\Delta O_2/Ar$ and [POC] was more tightly coupled during the second drifter deployment, with closer agreement between the two measures of NCP (Fig 3). Both O_2/Ar and [POC] displayed regular diurnal variations, increasing in the daytime and decreasing at night (Fig. S5a–b). Over the full drifter deployment, concentrations of Chl-a and, to a lesser extent, POC decreased, in contrast to $\Delta O_2/Ar$, which remained relatively constant across days. Values of $NCP_{O2/Ar}$ ranged from 26 to 33 mmol C m^{-2} d^{-1} over two consecutive 24 hour periods, while NCP_{POC} values ranged from -3 to 1 mmol C m^{-2} d^{-1} (Fig. 4). NPP based on the CbPM calculations was 22 mmol C m^{-2} d^{-1} on the first day of the drifter period and 18 mmol C m^{-2} d^{-1} on the second day, while NPP calculated from one ^{14}C bottle incubation during the first day of the drifter 2 deployment was 12 ± 4 mmol C m^{-2} d^{-1}, showing reasonably good agreement with values derived from the CbPM calculations (Table 1).

4 Discussion

The results from our Lagrangian surveys illustrate diurnal dynamics in two contrasting productivity regimes off the Oregon coast. Biogeochemical properties during the first drifter deployment suggested a dynamic, highly productive phytoplankton community, influenced by upwelling and elevated mixed layer nutrient concentrations (Figs. 1, S3). Several lines of evidence imply the presence of a developing diatom bloom at this site. Increasing mixed layer biological oxygen saturation ($\Delta O_2/Ar$) was contrasted by a general decrease in particulate organic carbon (POC) concentrations, suggesting a significant decoupling between O_2 and POC dynamics. In contrast, biogeochemical properties during the second drifter deployment were indicative of a lower productivity, nutrient-limited phytoplankton assemblage, with near-zero $\Delta O_2/Ar$ values reflecting a close balance between water column photosynthesis and respiration (Fig. 3a). Relative to the drifter 1 site, diurnal variations in $\Delta O_2/Ar$ and POC were more closely coupled, while phytoplankton biomass (C_{ph}) and chlorophyll-a (Chl-a) concentrations (dominated by smaller cells) varied little through time. The contrasting properties between the two drifter deployments enable us to examine the coupling of O_2 and POC dynamics under different ecological states, with implications for the use of $\Delta O_2/Ar$ and POC measurements as proxies for NCP.

4.1 Decoupling of NCP and POC dynamics in the mixed layer

4.1.1. Drifter 1

In the absence of significant POC sinking and net loss to the dissolved organic carbon (DOC) pool, NCP_{POC} should approximate $NCP_{O2/Ar}$ (Claustre et al., 2008; White et al., 2017). However, over the three successive 24-hour periods of drifter deployment 1, $NCP_{O2/Ar}$ values were consistently higher than NCP_{POC}, with the absolute difference increasing from 79 mmol C m^{-2} d^{-1} to 175 mmol C m^{-2} d^{-1} and exceeding the propagated uncertainties of each NCP measure during days two to three (Fig. 4; Table 1). The increasingly negative NCP_{POC} values over the course of the drifter 1 deployment primarily reflect diminishing rates of POC accumulation (dPOC/dt term in Eq. (8)) in the daytime (Fig. S5). Likewise, we found that gross daily increases

in POC (i.e., gross primary production, or GPP) were significantly lower than increases in $[O_2]_{bio}$, corrected for gas exchange and/or mixing, during days two to three of the drifter period (Table 1). The differences in magnitude of daily decreases in POC and $[O_2]_{bio}$, corrected for gas exchange and/or mixing (i.e., community respiration), were generally smaller and often closer in magnitude to the uncertainty of both measurements. Thus, the discrepancy between NCP measures was more attributable to differences in gross accumulation of POC and O_2 (Claustre et al., 2008; White et al., 2017), rather than differences in POC and O_2 losses.

Additional constraints on NCP can be derived from examining nutrient budgets. Because vertical upwelling of nutrient-replete waters would dampen the magnitude of observed nutrient drawdown over time (Sect. 3.1), we used the derived k_{mix} from Eq. 6 and a best-fit vertical gradient in nutrient concentrations between the mixed layer and 100 m (Sect. 2.4) to account for this mixing effect. This correction increases the cumulative three-day nutrient drawdown by 2-3 times. Over the three-day drifter deployment (Sect. 3.1), surface Si, N and P concentrations declined in a ratio of 17: 13: 1, which is consistent with the stoichiometry expected for organic matter produced by a diatom-rich assemblage (Brzezinski et al., 1998; Turner et al., 1998; Brzezinski, 2004). Assuming that the observed decrease in SiO_2 concentrations over the three days is attributable to export of diatomaceous particles out of the mixed layer, and applying a stoichiometric ratio of 106 C: 16 Si, we estimate an average C fixation rate of ~132 mmol C m^{-2} d^{-1} for the drifter period. This value is consistent with $NCP_{O2/Ar}$ (Table 1) but significantly greater than NCP_{POC} estimates. Taken together, these comparisons among $NCP_{O2/Ar}$, NCP_{POC} and the average daily nutrient drawdown rate suggest that additional POC losses decoupled O_2 from POC dynamics during the drifter period. While mixed layer $\Delta O_2/Ar$ was primarily impacted by the accumulation of O_2 from gross primary production (GPP) and O_2 loss from community respiration, diurnal variability in [POC] was also likely affected by several additional loss factors, including particle export, photooxidation, grazing, and DOC production.

During a diatom bloom, enhanced aggregation of large silica-rich particles and zooplankton fecal pellet production can stimulate export of POC and diatom cells out of the mixed layer, progressively decreasing NCP_{POC} values relative to $NCP_{O2/Ar}$. A number of previous studies have reported enhanced particle fluxes associated with diatoms blooms in various oceanic regions (Buesseler, 1998; Guidi et al., 2009; Brzezinski et al., 2015; Stukel et al., 2017) . The global compilation of Henson et al. (2012) reported maximum export fluxes of ~83 mmol C m^{-2}

d^{-1} from Southern Ocean measurements, while Alkire et al. (2012) observed maximum export fluxes of 96 mmol C m^{-2} d^{-1} during termination of the North Atlantic spring bloom. Stukel et al. (2017) applied the steady-state ^{234}Th-^{238}U approach to quantify export fluxes of ~36 mmol C m^{-2} d^{-1} in the nearshore region of the Southern California Current system. The upper values of these estimates are in the range of the discrepancy we measured between NCP_{POC} and $NCP_{O2/Ar}$, suggesting that POC export fluxes could potentially account for a significant fraction of the inferred POC loss at drifter site 1.

Another likely POC loss is DOC production through cellular exudation, viral lysis and/or grazing (Briggs et al., 2018; Claustre et al., 2008; Dall'Olmo et al., 2011; Lochte et al., 1993). Loss of POC to the DOC pool would lower NCP_{POC} without affecting $NCP_{O2/Ar}$ values if the DOC produced is not respired in the mixed layer. While we did not conduct direct measurements of DOC concentrations during the cruise, previous work in a variety of ocean environments has shown that DOC production can account for 3-37% of NCP in the Ross Sea, up to 10-40% in the equatorial Pacific Ocean, and up to 66% in the Sargasso Sea during the seasonal phytoplankton bloom (Hansell and Carlson, 1998). More recently, Alkire et al. (2012) estimated that 22-40% of NCP was released into the DOC pool during the North Atlantic bloom, and Bif and Hansell (2019) estimated springtime ΔDOC/NCP ratios of 0.05 – 0.54 and summertime ratios of 0 – 0.28 along the Line P transect (130 – 152 °W) in the eastern Subarctic Pacific. The closest Line P measurement to drifter station 1 in terms of location and [Chl-a] exhibited a ΔDOC/NCP ratio of 0.19 in the summer and 0.34 in the spring, implying that up to 34% of NCP was partitioned into the DOC pool. Assuming a lower bound of ~20% of NCP released as DOC yields a daily-integrated DOC flux of 20 to 33 mmol C m^{-2} d^{-1}. The remaining discrepancy between $\Delta O_2/Ar$ and POC-based NCP estimates, 50 to 142 mmol C m^{-2} d^{-1} (average = 100 mmol C m^{-2} d^{-1}) is potentially attributable to export flux. Taking an upper bound of 40% of NCP as DOC production, which is closer to the easternmost station sampled in Bif and Hansell (2019), yields a daily-integrated DOC flux of 40 to 66 mmol C m^{-2} d^{-1} (Fig. 4) and a residual export flux of 21 to 108 mmol C m^{-2} d^{-1} (average = 73 mmol C m^{-2} d^{-1}). These results demonstrate that applying a reasonable range of ΔDOC/NCP values does not change our conclusion that export fluxes comprise a significant proportion of the discrepancy between NCP measures at drifter site 1.

A final consideration involves diurnal variation of zooplankton abundances and grazing rates, which may introduce an additional POC loss process decoupling mixed layer POC/C_{ph} and

dissolved ΔO_2 dynamics (Dall'Olmo et al., 2011; Briggs et al., 2018). During our expedition, we observed a strong signature of diel migrating zooplankton based on increased night-time signal spikes in surface optical backscatter measurements (Burt and Tortell, 2018). In addition to particle sinking and DOC excretion, these nighttime migrations could enhance POC and C_{ph} loss at night without depleting ΔO_2/Ar, if POC uptake rates exceed respiration rates. For example, (Wu et al., 2010) observed that mesozooplankton prefer to graze diatom-dominated assemblages at night over day in the East China Sea. Assuming that biomass accumulation rates from grazing surpasses grazer respiration rates (Dagg et al., 1982), these diurnal variations would contribute to more POC loss than O_2 loss. In addition, once POC is assimilated into the body of a grazer, it joins a larger particle size class that likely exceeds the size-dependent detection limits of the beam attenuation coefficient (Stramski and Kiefer, 1991; Marra, 2002; Claustre et al., 2008;), decreasing the c_p signal used to derive POC.

4.1.2 Drifter 2. Compared to drifter site 1, absolute differences in $NCP_{O2/Ar}$ and NCP_{POC} estimates were consistently smaller at drifter site 2, ranging from 28 to 32 mmol C $m^{-2}d^{-1}$ over two 24-hour periods (Fig. 4). These differences still exceed the uncertainty in each NCP calculation. As during drifter period 1, differences between ΔO_2/Ar and POC-derived GPP, corrected for mixing and/or gas exchange, contributed more to the apparent NCP discrepancy than differences in ΔO_2/Ar and POC-derived respiration rates (Table 1). Overall, the closer absolute agreement across NCP estimates is consistent with the view of drifter site 2 as a more oligotrophic ecosystem, where primary production and heterotrophic consumption are more tightly coupled (Claustre et al., 2008; White et al., 2017). Such a coupling between phytoplankton production and loss through mortality and predation acts to dampen variability in phytoplankton biomass and NCP.

The smaller absolute differences between $NCP_{O2/Ar}$ and NCP_{POC} suggest a lower potential for POC sinking, DOC production and grazing to decouple POC, C_{ph} and ΔO_2/Ar dynamics at drifter site 2. Although we lack direct DOC measurements, lower 440 nm absorption values in the filtration blanks (Sect. 2.2) at drifter site 2 compared to drifter site 1 suggest lower colored dissolved organic matter (CDOM) concentrations (Organelli et al., 2014; Peacock et al., 2014). This observation is consistent with several previous observations of lower DOC production in lower productivity and/or oligotrophic waters (Bif et al., 2018; Hansell and Carlson, 1998). A

recent compilation of summertime DOC production and NCP measurements along the Line P transect in the Northeast Pacific Ocean, shows that DOC production comprises at most 28% of total NCP in offshore waters (Bif and Hansell, 2019). Even DOC/NCP ratios as high as 28% at drifter site 2, would result in low overall DOC accumulation, because NCP rates were relatively low.

Low particle sinking rates are another factor that can explain the smaller absolute discrepancy between $NCP_{O2/Ar}$ and NCP_{POC} at drifter site 2. Low particle export is generally expected from phytoplankton assemblages dominated by small particle sizes <20μm, consistent with the higher b_{bp} slope values and Chl-a size fractionation measurements at drifter site 2 (Sect. 3.2; Fig. 2) (Fowler and Knauer, 1986; Guidi et al., 2008). Nonetheless, POC export does occur under low productivity conditions, and even small export fluxes could account for the entire discrepancy between measures of NCP at drifter site 2. For example, Durkin et al., (2015) reported significant rates of particle sinking from the small-celled, oligotrophic communities that dominate the BATS station. In addition, it is possible that grazing by zooplankton would also enhance loss of these phytoplankton cells from the mixed layer (Guidi et al., 2009). As we observed at drifter site 1, increased variability in the b_{bp} signal suggest the presence of vertically migrating zooplankton into the mixed layer during nighttime intervals of drifter period 2 (Burt and Tortell, 2018). Assuming 28% of $NCP_{O2/Ar}$ is DOC production at drifter site 2, a residual POC export flux of 21 to 23 mmol C m^{-2} d^{-1} would be necessary to balance $NCP_{O2/Ar}$ and NCP_{POC}. This value is reasonable considering previous estimates reported from a number of lower productivity systems (Henson et al., 2012; Charette et al., 1999).

4.2 Other factors driving variability in NCP_{POC}

In interpreting our results, it is important to consider a number of potential caveats, including methodological uncertainties and other POC sinks that could contribute to the variability in derived NCP estimates, POC export and DOC excretion rates. In our analysis, we interpret variations in particulate backscatter (b_{bp}) and beam attenuation (c_p) in terms of phytoplankton and total particulate organic carbon concentrations, assuming a small influence of inorganic suspended minerals from the continental shelf, Columbia River discharge or other sources. However, the Columbia River plume has been observed to extend south along the coast

as far as ~44.5° N in the summertime (Thomas and Weatherbee, 2006), close to the location of drifter deployment 1. Moreover, the drifter was deployed ~40 km from shore over the continental shelf, where bottom resuspension of particles and their subsequent upwelling into the mixed layer is possible. Estimates of the bulk refractive index of particles (η_p), can be used to estimate the influence of inorganic minerals in our optical measurements. During drifter deployment 1, we observed median η_p values at 470, 532 and 650 nm that were generally below 1.12 (Fig. S3e), whereas inorganic minerals in seawater, have a bulk refractive index as high as 1.26 (Lide, 1997; Twardowski et al., 2001). In addition, mixing with the fresh Columbia River plume would have significantly reduced salinity at drifter site 1 to values below 30 g/kg (Hickey et al., 1998), well below the 32 g/kg we observed during this drifter deployment (Sect. 3.1; Fig. S3c), which are consistent with salinities observed in the offshore Northeast Pacific Ocean (Whitney and Freeland, 1999). While these relatively high salinities support our assertion of a negligible influence of riverine particles on our measurements, the observed η_p values do not preclude the presence of mixing between POC and a small fraction of shelf-derived inorganic particles at drifter site 1. By contrast, calculated η_p values during deployment 2 were below 1.08, which is close to values expected for water-containing predominantly non-diatom phytoplankton organic carbon.

Additional uncertainty in our analysis derives from the algorithms used to estimate POC and phytoplankton carbon C_{ph} from optical measurements (Sect. 2.2). Because of particle size limitations in the optical measurements, variability in seawater optical properties may not fully capture all significant components of the particulate pool, such as larger microplankton and zooplankton. Indeed, larger zooplankton often appear as erratic signal spikes in backscatter data (Burt and Tortell, 2018), which are typically filtered out during data processing. Moreover, the c_p signal at 660 nm, used to derive [POC], responds most strongly to particles within the 0.5–20 µm diameter range (Claustre et al., 2008; Marra, 2002; Stramski and Kiefer, 1991), which is smaller than many large diatoms, fecal pellets and particle aggregates. This size bias would cause an underestimate of larger particles, and therefore [POC], measured by beam attenuation, thereby contributing to the apparent discrepancy between diel changes in [POC] and diel changes in $\Delta O_2/Ar$ (Fig. 4). Despite these potential caveats, recent work (Graff et al., 2016; Briggs et al., 2018; Burt et al., 2018) has demonstrated that c_p and b_{bp}-based derivations of [POC] and [C_{ph}]

720 can indeed be robust in high biomass ocean regions, where productivity and the proportion of
721 large-celled phytoplankton may be greater.
722 Changes in the c_p-to-[POC] relationship through time could also drive apparent
723 variability in our optical [POC] estimates during both drifter deployments. On a global scale, the
724 linear regression of [POC] against c_p at 660 nm measured in samples from diverse marine
725 environments is defined over a range of POC concentrations from ~5 to ~175 µg/L (Graff et al.
726 2015). At drifter site 2, the POC concentrations fell within the range of this fit. The assumption
727 of a constant POC/c_{p660} ratio close to the value suggested by Graff et al. (2015), is less likely to
728 impact the derivation of apparent POC standing stocks and associated NCP estimates. Based on
729 relatively small changes in b_{bp} slope values (Figs. S3d, S5d) and phytoplankton community
730 composition, it is unlikely that changes in particle size and bulk refractive index would have
731 significantly shifted the relationship between POC and c_{p660} during drifter deployment 2.
732 As concentrations of POC at drifter station 1 were 25% higher than the empirical limits
733 of the c_p-based algorithm in (Graff et al., 2015), a different POC/c_p relationship (i.e., different
734 slope of the linear fit) could apply. In a limited comparison with discrete POC samples, we found
735 a POC–c_p slope that was similar to that of Graff et al. (albeit with a different y intercept) (Fig.
736 S2). Nonetheless, we cannot rule out changes in the c_{p660}–[POC] relationship due to shifts in cell
737 size and, to a lesser extent, bulk refractive index resulting from diatom accumulation
738 (Kheireddine and Antoine, 2014; Stramski and Reynolds, 1993) (Fig. S3d–e). Indeed, Briggs et
739 al. (2018) observed that the ratio of [POC] to c_p decreased by ~20% during the rise of the North
740 Atlantic bloom, while values increased by ~60% during the bloom decline. If we assume a 20%
741 decrease in POC/c_{p660} values (from ~420 to ~340 mg m^{-2}) associated with diatom growth (Briggs
742 et al., 2018), our daily NCP_{POC} estimates would be closer to 0, less positive during day 1 and less
743 negative during days 2–3. This, in turn, would increase the apparent decoupling between NCP_{POC}
744 and $NCP_{O2/Ar}$ on day 1, and bring the values slightly closer on days 2–3. The value of these
745 potential changes is small (<10%) relative to the differences we observed between $NCP_{O2/Ar}$ and
746 NCP_{POC}, and we thus conclude that variable POC/c_{p660} ratios cannot explain the observed
747 decoupling between POC, C_{ph} and dissolved O_2 dynamics at the drifter 1 site.
748 Finally, error associated with the POC mixing correction could affect calculated NCP_{POC}
749 values (Eq. 8) and therefore the discrepancy between $NCP_{O2/Ar}$ and NCP_{POC}, and derived export
750 estimates. This vertical mixing correction for NCP_{POC} is based on average parameters derived

751 from N_2O measurements for the whole drifter period (Sect. 2.5). This introduces some error in
752 day-to-day corrections to the NCP_{POC} calculations. In addition, the gradient term dPOC/dz in Eq.
753 9 is based on the difference between average POC concentrations measured at two depths during
754 CTD deployments (5 m and one depth over 40-60 m). Because high-resolution transmissivity
755 profiles showed that particle concentrations reached a steady minimum between 30 m and 40 m
756 in most CTD deployments, dz in Eq. 9 was taken as the difference between the drifter 1 z_{mld} and
757 ~32 m (averaged across transmissivity profiles), rather than deeper POC sampling depth (i.e., 40
758 – 60 m). Because variations in transmissivity do not necessarily equate to variations in [POC],
759 errors in dz would impact the vertical mixing correction and therefore calculated NCP_{POC} values.
760 For example, if the [POC] minimum was actually deeper, this would increase the value of dz and
761 decrease dPOC/dz and the total mixing correction, yielding lower NCP_{POC} values and a higher
762 discrepancy between NCP measures. In propagating the error for NCP_{POC}, we have included an
763 error of ± 7 m to partially address this uncertainty in the POC minimum depth, based on the
764 variability in minimum transmissivity during drifter period 1. Fortunately, the cumulative
765 NCP_{POC} mixing corrections over the three-day drifter period approximate the cumulative
766 magnitude of the N_2O-based $NCP_{O2/Ar}$ mixing correction (sum three values for the N_2O and POC
767 mixing correction in Table 1), increasing our confidence in the POC mixing correction applied
768 here.

769 Aside from uncertainties that directly impact estimates of NCP, there are a number of
770 other potential caveats in our analysis of phytoplankton carbon from b_{bp} and particle size
771 distribution from b_{bp} slope. Previous studies have reported that daily variations in b_{bp} do not
772 always track daily variations in c_p, suggesting that b_{bp} dynamics do not reflect phytoplankton
773 carbon dynamics on diel time scales (Kheireddine and Antoine, 2014; Briggs et al. 2018). We
774 observed a similar decoupling between b_{bp} and c_p in this study; for example, while c_p values at
775 660 nm steadily declined in the last 24 hours of drifter period 1, b_{bp} at 470 nm stayed relatively
776 constant. Nonetheless, [C_{ph}] estimates from b_{bp} (Fig. 2) remain useful for comparisons between
777 drifter sites, and differences in apparent phytoplankton biomass concentration were consistent
778 with a number of the other biogeochemical differences measured between the two trophic
779 regimes. Similarly, the relationship between b_{bp} slope and particle size distribution has been
780 challenged in previous literature (e.g., Zeng et al., 2018). While this limits our interpretation of
781 daily b_{bp} slope dynamics, we did find independent evidence for larger particle sizes at drifter site

1 (as predicted by the b_{bp} slope), from size fractionated Chl-a measurements and pigment analysis showing a greater fraction of diatoms (Sect. 3.2).

4.3 Reconciling NCP and NPP

During both drifter surveys, we estimated daily-integrated net primary productivity (NPP) values using carbon-based productivity model (CbPM) calculations and ^{14}C bottle incubations (Sect. 2.5). On several days, these two measures of NPP estimates were consistently lower than $NCP_{O2/Ar}$ integrated over the same time scales and mixed layer depths (Table 1; Fig. 4). Similarly, Briggs et al. (2018) and Alkire et al. (2012) also reported NCP values that were equal to or greater than NPP values obtained from different methodologies during their Lagrangian study of the North Atlantic Bloom. Oxygen-based GPP and daytime rates of net accumulation in $\Delta O_2/Ar$, based on change in $[O_2]_{bio}$, corrected for mixing and gas exchange and then normalized to a photosynthetic quotient of 1.4 (Sect. 2.6, Claustre et al. 2008; White et al. 2017), were significantly higher than NPP, as well (Table 1).

In theory, this result is impossible, as NCP includes additional respiration terms not included in NPP, and must always be equal to or (more realistically) lower than NPP. Recent work in the Northeast Pacific Ocean, has reported mean NCP/NPP ratios, based on $\Delta O_2/Ar$ measurements and CbPM calculations, in the 0.16 to 0.26 range for offshore and coastal waters, respectively (Burt et al., 2018). These values, determined from continuous observations along a moving ship-track are consistent with theoretical expectations. The observed low apparent NPP/NCP values observed in our study and that of Briggs et al. (2018) and Alkire et al. (2012) highlight a number of methodological limitations that could depress NPP estimates.

One possibility, which has been discussed at length by various authors (Gieskes et al., 1979; Fogg and Calvario-Martinez, 1989; Marra, 2009), is that bottle containment effects limit accurate estimates of ^{14}C uptake. This likely caused underestimates of ^{14}C-NPP during both drifter surveys, relative to CbPM-NPP and $NCP_{O2/Ar}$. In addition, during this last ^{14}C-uptake experiment of drifter survey 2, the incubator warmed significantly, which could have significantly impacted phytoplankton growth rates during the incubation and result in depressed ^{14}C-NPP values (Eppley, 1968).

A number of factors may also depress CbPM-based NPP estimates. While the model applies a satellite-based relationship between [Chl-a]/[C_{ph}] and daily mixed layer irradiance (E_g) to calculate growth rate, these E_g values may not fully parametrize phytoplankton physiology for mixed assemblages in the ocean (Westberry et al., 2008). Indeed, phytoplankton photophysiology varies with other environmental conditions and phytoplankton composition (Cloern et al., 1995; Geider et al., 1998; MacIntyre et al., 2002; Westberry et al., 2008). In addition, the CbPM does not allow calculated growth rates to exceed 2 d^{-1}, which may not apply to all ocean environments (Graff et al., 2016). These uncertainties could potentially impact the applicability of the CbPM parameters to the specific ocean conditions at drifter sites 1 and 2. In addition, a vertical mixing correction for ac-s and backscatter-derived [Chl-a] and [C_{ph}], respectively, not feasible in the present data set, may improve CbPM-based estimates of NPP.

4.4 Comparison to other studies

A number of previous studies have examined diurnal variation in upper ocean phytoplankton and organic particle dynamics across a variety of productivity regimes, from oligotrophic environments (Claustre et al., 1999, 2008; Wu et al., 2010; Gernez et al., 2011; Kheireddine and Antoine, 2014; Thyssen et al., 2014; Nicholson et al., 2015; Ribalet et al., 2015; White et al., 2017), to higher productivity waters and phytoplankton blooms (Brunet and Lizon, 2003; Wu et al., 2010; Alkire et al., 2012; Gernez et al., 2011; Dugenne et al., 2014; Kheireddine and Antoine, 2014; Needham and Fuhrman, 2016; Briggs et al., 2018). In general, these studies have shown that more productive environments exhibit higher amplitude diurnal variations in beam attenuation, POC concentration, phytoplankton cell abundances, Chl-a, and metabolic rates, as compared to oligotrophic regions. These prior results are consistent with the differences we observed between the two distinct Northeast Pacific trophic environments represented by drifter sites 1 and 2, respectively (Figs. 2; S4).

To our knowledge, however, only two previous studies have directly compared diurnal variations in O_2-based and c_p-based mixed layer productivity using Lagrangian drifters (Alkire et al., 2012; Briggs et al., 2018). This previous work demonstrated that GPP and NCP dynamics derived from dissolved O_2 measurements differed from net POC accumulation over the course of the North Atlantic bloom, with the magnitude of this disparity varying as a function of bloom

stage. The authors found that highest rates of POC export and DOC production, corresponding to the greatest O_2-POC discrepancy, occurred during the main period of the bloom development, prior to its termination. The results of our study off the Oregon coast extend these previous observations from the North Atlantic bloom into two new surface ocean regimes: a high productivity Pacific upwelling zone, and lower productivity offshore region. The upwelling environment was characterized by rapid diatom accumulation, yielding significant differences between $NCP_{O2/Ar}$ and NCP_{POC}, as observed at the height of the North Atlantic bloom. In contrast, the lower productivity drifter 2 site exhibited tighter coupling between POC and O_2 dynamics, and daily-integrated measures of NCP and net carbon accumulation.

Our results overall support the continued use of diurnal measurements of beam attenuation to estimate NCP_{POC} in low productivity regimes, where POC and O_2 dynamics are closely coupled. However, in support of findings from the North Atlantic Bloom (Alkire et al., 2012; Briggs et al., 2018), measurements of both POC and O_2 are likely required to constrain organic carbon mass balance in higher productivity regions, where POC and O_2 dynamics can be significantly uncoupled on short time scales. Contrary to our expectations, even lower productivity environments like drifter site 2 can display a quantifiable, though smaller discrepancy between NCP measures, as well. Measurements that simultaneously estimate surface water O_2 accumulation, net DOC production and vertical transport of deep water to the mixed layer at high temporal resolution offer the opportunity to evaluate the fate of NCP. These quantities are especially important in the California coastal upwelling regime and other similar ecosystems, with high NCP and significant potential for carbon transfer to higher trophic levels.

5 Conclusions

In the current study, biological oxygen saturation ($\Delta O_2/Ar$) and optically-derived particulate organic carbon (POC) were measured continuously and simultaneously during two Lagrangian drifter deployments. This dual measurement approach allowed us to examine the (de)coupling between carbon and dissolved oxygen in surface waters, and facilitated direct comparison of O_2/Ar and POC-derived measures of gross primary productivity (GPP), community respiration, and net community production (NCP). The deployment of the drifters in contrasting hydrographic regimes allowed us to assess and compare the diurnal variations of O_2

and POC across a productivity gradient, from a mesotrophic upwelling-influenced system, to an oligotrophic system further offshore. As hypothesized, the results suggest that O_2 and POC-based measures of NCP diverge in mid-to-high productivity phytoplankton communities, where daily fluctuations in $\Delta O_2/Ar$ are decoupled from POC cycling. In contrast, the two NCP estimates showed better agreement in lower productivity regions, where O_2 and POC cycles appeared to be more tightly coupled. These findings are consistent with current understanding of productivity dynamics in these two coastal Pacific environments, and complement the only prior comparison of daily GPP and NCP estimates from simultaneous, autonomous measurements of c_p and O_2 in the North Atlantic mixed layer (Alkire et al., 2012; Briggs et al., 2018). We have further shown that for upwelling regions like drifter site 1, it is important to account for vertical mixing of sub-surface waters into the mixed layer, and its effect on not only $NCP_{O2/Ar}$ calculations (Izett et al., 2018), but also on NCP_{POC} estimates through dilution of the surface POC signature. Thus, our study illustrates an application of the vertical mixing coefficient, k_{mix}, derived from $[N_2O]$ profiles, to more accurately estimate net changes in POC and nutrient concentration in such environments.

Moving forward, the disparity between POC and O_2-based NCP estimates offers an opportunity to continuously track POC fate in the mixed layer using autonomous ship-board or in situ sensors. The results show that this approach performs well in distinguishing regions of high particle export, notwithstanding some major methodological limitations (Sect. 4.2), and poorly constrained DOC production rates (Sect. 4.1.1), which increase the uncertainty of our export estimates at drifter site 1 (Fig. 4). As it is difficult and labor intensive to measure POC export on short time scales with sediment traps and the ^{234}Th-^{238}U disequilibrium method (Buesseler et al., 2006; Savoye et al., 2006), simultaneous underway measurements of dissolved O_2, particulate beam attenuation and CDOM absorption and spectral slope over a range of wavelengths <400 nm (Del Vecchio and Blough, 2004; Grunert et al., 2018) may provide a valuable, first-order approximation of POC partitioning among living phytoplankton biomass, particle export and dissolved organic carbon (DOC) in the surface ocean on short time scales.

For future work, we recommend a number of approaches to increase our confidence in derived POC export from coupled O_2, POC, and DOC dynamics. First, it will be valuable to constrain particle size, and partitioning of POC into detrital and living (phytoplankton and heterotrophic bacteria) components to properly assess the size range captured by optics-based

POC and C_{ph} measurements. Second, independent estimates of POC export during each drifter deployment could validate estimates of POC export fluxes derived from coupled O_2 and POC measurements. Relatedly, depth-resolved backscatter profiles (Briggs et al., 2013, 2018) could be used as another autonomous approach to calculating export fluxes, as an independent check on surface-based estimates. Going forward, there is significant future potential to exploit coupled O_2 and c_p measurements on autonomous platforms, including various ocean moorings (e.g., the Optical Dynamics Experiment, the Biowatt II program, and the Bermuda Testbed Mooring program), and biogeochemical floats and gliders to resolve opportunistic, high-resolution POC export time series (Stramska and Dickey, 1992; Kinkade et al., 1999; Dickey and Chang, 2002). Deployment of such autonomous measurement systems across a range of oceanic regions will help to constrain POC and productivity dynamics on global scales.

Data availability

Discrete and underway optical measurements may be accessed at https://github.com/srosengard/rosengard-tortell-oc2017.git

Author contributions

Sarah Rosengard, Philippe Tortell, and Nina Schuback collected the data in the field. Robert Izett processed the CTD cast data and nitrous oxide measurements. Sarah Rosengard wrote the manuscript with significant input from the co-authors.

Competing interests

The authors declare that they have no conflict of interest.

Acknowledgements

Special thanks to Jessie Gwinn, Jay Pinckney, Ross McCulloch, Chen Zeng, Melissa Beaulac, Chris Payne and Maureen Soon for assistance in field collection and analysis of samples. This

project was funded by the Natural Sciences and Engineering Research Council of Canada (NSERC), and by the US National Science Foundation (NSF project number 1436344).

References

Alkire, M. B., D'Asaro, E., Lee, C., Jane Perry, M., Gray, A., Cetinić, I., Briggs, N., Rehm, E., Kallin, E., Kaiser, J. and González-Posada, A.: Estimates of net community production and export using high-resolution, Lagrangian measurements of O2, NO3−, and POC through the evolution of a spring diatom bloom in the North Atlantic, Deep Sea Res. Part I Oceanogr. Res. Pap., 64, 157–174, doi:10.1016/j.dsr.2012.01.012, 2012.

Behrenfeld, M. J., Boss, E., Siegel, D. A. and Shea, D. M.: Carbon-based ocean productivity and phytoplankton physiology from space, Global Biogeochem. Cycles, 19(1), 2005.

Bif, M. B. and Hansell, D. A.: Seasonality of dissolved organic carbon in the upper Northeast Pacific Ocean, Global Biogeochem. Cycles, 2019.

Bif, M. B., Hansell, D. A. and Popendorf, K. J.: Controls on the fate of dissolved organic carbon under contrasting upwelling conditions, Front. Mar. Sci., 5, 463, 2018.

Boss, E., Twardowski, M. S. and Herring, S.: Shape of the particulate beam attenuation spectrum and its inversion to obtain the shape of the particulate size distribution, Appl. Opt., 40(27), 4885–4893, 2001.

de Boyer Montégut, C., Madec, G., Fischer, A. S., Lazar, A. and Iudicone, D.: Mixed layer depth over the global ocean: An examination of profile data and a profile-based climatology, J. Geophys. Res., 109(C12), C12003, doi:10.1029/2004JC002378, 2004.

Briggs, N., Guðmundsson, K., Cetinić, I., D'Asaro, E., Rehm, E., Lee, C. and Perry, M. J.: A multi-method autonomous assessment of primary productivity and export efficiency in the springtime North Atlantic, Biogeosciences, 15(14), 4515–4532, 2018.

Briggs, N. T., Slade, W. H., Boss, E. and Perry, M. J.: Method for estimating mean particle size from high-frequency fluctuations in beam attenuation or scattering measurements, Appl. Opt., 52(27), 6710–6725, 2013.

Brunet, C. and Lizon, F.: Tidal and diel periodicities of size-fractionated phytoplankton pigment signatures at an offshore station in the southeastern English Channel, Estuar. Coast. Shelf Sci., 56(3–4), 833–843, 2003.

967 Brzezinski, M., Villareal, T. and Lipschultz, F.: Silica production and the contribution of diatoms
968 to new and primary production in the central North Pacific, Mar. Ecol. Prog. Ser., 167, 89–104,
969 doi:10.3354/meps167089, 1998.
970 Brzezinski, M. A.: The Si:C:N ratio of marine diatoms: Interspecific variability and the effect of
971 some environmental variables, J. Phycol., 21(3), 347–357, doi:10.1111/j.0022-
972 3646.1985.00347.x, 2004.
973 Brzezinski, M. A., Krause, J. W., Bundy, R. M., Barbeau, K. A., Franks, P., Goericke, R.,
974 Landry, M. R. and Stukel, M. R.: Enhanced silica ballasting from iron stress sustains carbon
975 export in a frontal zone within the California Current, J. Geophys. Res. Ocean., 120(7), 4654–
976 4669, 2015.
977 Buesseler, K. O.: The decoupling of production and particulate export in the surface ocean,
978 Global Biogeochem. Cycles, 12(2), 297–310, 1998.
979 Buesseler, K. O., Benitez-Nelson, C. R., Moran, S. B., Burd, A., Charette, M., Cochran, J. K.,
980 Coppola, L., Fisher, N. S., Fowler, S. W. and Gardner, W. D.: An assessment of particulate
981 organic carbon to thorium-234 ratios in the ocean and their impact on the application of 234Th as
982 a POC flux proxy, Mar. Chem., 100(3–4), 213–233, 2006.
983 Burt, W. J. and Tortell, P. D.: Observations of Zooplankton Diel Vertical Migration From High-
984 Resolution Surface Ocean Optical Measurements, Geophys. Res. Lett., 45(24), 13–396, 2018.
985 Burt, W. J., Westberry, T. K., Behrenfeld, M. J., Zeng, C., Izett, R. W. and Tortell, P. D.:
986 Carbon: Chlorophyll Ratios and Net Primary Productivity of Subarctic Pacific Surface Waters
987 Derived From Autonomous Shipboard Sensors, Global Biogeochem. Cycles, 32(2), 267–288,
988 doi:10.1002/2017GB005783, 2018.
989 Capelle, D. W., Dacey, J. W. and Tortell, P. D.: An automated, high through-put method for
990 accurate and precise measurements of dissolved nitrous-oxide and methane concentrations in
991 natural waters, Limnol. Oceanogr. Methods, 13(7), 345–355, 2015.
992 Cassar, N., Barnett, B. A., Bender, M. L., Kaiser, J., Hamme, R. C. and Tilbrook, B.: Continuous
993 high-frequency dissolved O2/Ar measurements by equilibrator inlet mass spectrometry, Anal.
994 Chem., 81(5), 1855–1864, 2009.
995 Cassar, N., Nevison, C. D. and Manizza, M.: Correcting oceanic O2/Ar-net community
996 production estimates for vertical mixing using N2O observations, Geophys. Res. Lett., 41(24),
997 8961–8970, 2014.

Charette, M. A., Moran, S. B. and Bishop, J. K. B.: 234Th as a tracer of particulate organic carbon export in the subarctic northeast Pacific Ocean, Deep Sea Res. Part II Top. Stud. Oceanogr., 46(11-12), 2833-2861, 1999.

Claustre, H., Morel, A., Babin, M., Cailliau, C., Marie, D., Marty, J., Tailliez, D. and Vaulot, D.: Variability in particle attenuation and chlorophyll fluorescence in the tropical Pacific: Scales, patterns, and biogeochemical implications, J. Geophys. Res. Ocean., 104(C2), 3401–3422, 1999.

Claustre, H., Huot, Y., Obernosterer, I., Gentili, B., Tailliez, D. and Lewis, M.: Gross community production and metabolic balance in the South Pacific Gyre, using a non intrusive bio-optical method, Biogeosciences, 5, 463-474, 2008.

Cloern, J. E., Grenz, C. and Vidergar-Lucas, L.: An empirical model of the phytoplankton chlorophyll: carbon ratio-the conversion factor between productivity and growth rate, Limnol. Oceanogr., 40(7), 1313–1321, 1995.

Dagg, M. J., Vidal, J., Whitledge, T. E., Iverson, R. L. and Goering, J. J.: The feeding, respiration, and excretion of zooplankton in the Bering Sea during a spring bloom, Deep Sea Res. Part A. Oceanogr. Res. Pap., 29(1), 45–63, 1982.

Dall'Olmo, G., Boss, E., Behrenfeld, M. J., Westberry, T. K., Courties, C., Prieur, L., Pujo-Pay, M., Hardman-Mountford, N. and Moutin, T.: Inferring phytoplankton carbon and eco-physiological rates from diel cycles of spectral particulate beam-attenuation coefficient, Biogeosciences, 8(11), 3423–3439, 2011.

Del Vecchio, R., and Blough, N. V.: Spatial and seasonal distribution of chromophoric dissolved organic matter and dissolved organic carbon in the Middle Atlantic Bight, Mar. Chem., 89(1-4), 169-187, 2004.

Dickey, T. D. and Chang, G. C.: Recent advances and future visions: temporal variability of optical and bio-optical properties of the ocean, Oceanogr. DC-OCEANOGRAPHY Soc., 14(3), 15–29, 2002.

Dugenne, M., Thyssen, M., Nerini, D., Mante, C., Poggiale, J.-C., Garcia, N., Garcia, F. and Grégori, G. J.: Consequence of a sudden wind event on the dynamics of a coastal phytoplankton community: an insight into specific population growth rates using a single cell high frequency approach, Front. Microbiol., 5, 485, 2014.

Durkin, C. A., Estapa, M. L. and Buesseler, K. O.: Observations of carbon export by small sinking particles in the upper mesopelagic, Mar. Chem., 175, 72–81,

doi:10.1016/J.MARCHEM.2015.02.011, 2015.
Eppley, R. W.: An incubation method for estimating the carbon content of phytoplankton in natural samples, Limnol. Oceanogr., 13(4), 574–582, doi:10.4319/lo.1968.13.4.0574, 1968.
Fogg, G. E. and Calvario-Martinez, O.: Effects of bottle size in determinations of primary productivity by phytoplankton, Hydrobiologia, 173(2), 89–94, doi:10.1007/BF00015518, 1989.
Fowler, S. W. and Knauer, G. A.: Role of large particles in the transport of elements and organic compounds through the oceanic water column, Prog. Oceanogr., 16(3), 147–194, doi:10.1016/0079-6611(86)90032-7, 1986.
Garcia, H. E. and Gordon, L. I.: Oxygen solubility in seawater: Better fitting equations, Limnol. Oceanogr., 37(6), 1307–1312, 1992.
Gardner, W. D., Walsh, I. D. and Richardson, M. J.: Biophysical forcing of particle production and distribution during a spring bloom in the North Atlantic, Deep Sea Res. Part II Top. Stud. Oceanogr., 40(1–2), 171–195, 1993.
Geider, R. J., Maclntyre, H. L. and Kana, T. M.: A dynamic regulatory model of phytoplanktonic acclimation to light, nutrients, and temperature, Limnol. Oceanogr., 43(4), 679–694, 1998.
Gernez, P., Antoine, D. and Huot, Y.: Diel cycles of the particulate beam attenuation coefficient under varying trophic conditions in the northwestern Mediterranean Sea: Observations and modeling, Limnol. Oceanogr., 56(1), 17–36, 2011.
Gieskes, W. W. C., Kraay, G. W. and Baars, M. A.: Current 14C methods for measuring primary production: Gross underestimates in oceanic waters, Netherlands J. Sea Res., 13(1), 58–78, doi:10.1016/0077-7579(79)90033-4, 1979.
Graff, J. R., Westberry, T. K., Milligan, A. J., Brown, M. B., Dall'Olmo, G., Dongen-Vogels, V. van, Reifel, K. M. and Behrenfeld, M. J.: Analytical phytoplankton carbon measurements spanning diverse ecosystems, Deep Sea Res. Part I Oceanogr. Res. Pap., 102, 16–25, doi:10.1016/J.DSR.2015.04.006, 2015.
Graff, J. R., Westberry, T. K., Milligan, A. J., Brown, M. B., Olmo, G. D., Reifel, K. M. and Behrenfeld, M. J.: Photoacclimation of natural phytoplankton communities, Mar. Ecol. Prog. Ser., 542, 51–62, 2016.
Grunert, B. K., Mouw, C. B., and Ciochetto, A. B.: Characterizing CDOM spectral variability across diverse regions and spectral ranges, Global Biogeochem. Cycles, 32(1), 57-77, 2018.
Guidi, L., Jackson, G. A., Stemmann, L., Carlos Miquel, J., Picheral, M. and Gorsky, G.:

Author's personal copy Relationship between particle size distribution and flux in the mesopelagic zone, , doi:10.1016/j.dsr.2008.05.014, 2008.

Guidi, L., Stemmann, L., Jackson, G. A., Ibanez, F., Claustre, H., Legendre, L., Picheral, M. and Gorskya, G.: Effects of phytoplankton community on production, size, and export of large aggregates: A world-ocean analysis, Limnol. Oceanogr., 54(6), 1951–1963, 2009.

Hamme, R. C., Cassar, N., Lance, V. P., Vaillancourt, R. D., Bender, M. L., Strutton, P. G., Moore, T. S., DeGrandpre, M. D., Sabine, C. L. and Ho, D. T.: Dissolved O2/Ar and other methods reveal rapid changes in productivity during a Lagrangian experiment in the Southern Ocean, J. Geophys. Res. Ocean., 117(C4), 2012.

Hansell, D. A. and Carlson, C. A.: Net community production of dissolved organic carbon, Global Biogeochem. Cycles, 12(3), 443–453, 1998.

Henson, S. A., Sanders, R. and Madsen, E.: Global patterns in efficiency of particulate organic carbon export and transfer to the deep ocean, Global Biogeochem. Cycles, 26(1), 2012.

Hickey, B. M., Pietrafesa, L. J., Jay, D. A. and Boicourt, W. C.: The Columbia River plume study: Subtidal variability in the velocity and salinity fields, J. Geophys. Res. Ocean., 103(C5), 10339–10368, 1998.

Hirata, T., Hardman-Mountford, N. J., Brewin, R. J. W., Aiken, J., Barlow, R., Suzuki, K., Isada, T., Howell, E., Hashioka, T. and Noguchi-Aita, M.: Synoptic relationships between surface Chlorophyll-a and diagnostic pigments specific to phytoplankton functional types, Biogeosciences, 8(2), 311–327, 2011.

Hopkinson, B. M., and Barbeau, K.A.: Organic and redox speciation of iron in the eastern tropical North Pacific suboxic zone, Mar. Chem., 106(1-2), 2-17, 2007.

Hoppe, C. J. M., Schuback, N., Semeniuk, D. M., Maldonado, M. T. and Rost, B.: Functional Redundancy Facilitates Resilience of Subarctic Phytoplankton Assemblages toward Ocean Acidification and High Irradiance , Front. Mar. Sci. , 4, 229 [online] Available from: https://www.frontiersin.org/article/10.3389/fmars.2017.00229, 2017.

Izett, R. W., Manning, C. C., Hamme, R. C. and Tortell, P. D.: Refined estimates of net community production in the Subarctic Northeast Pacific derived from ΔO2/Ar measurements with N2O-based corrections for vertical mixing, Global Biogeochem. Cycles, 32(3), 326–350, 2018.

Jin, X., Najjar, R. G., Louanchi, F. and Doney, S. C.: A modeling study of the seasonal oxygen

budget of the global ocean, J. Geophys. Res. Ocean., 112(C5), 2007.
Kaiser, J., Reuer, M. K., Barnett, B. and Bender, M. L.: Marine productivity estimates from continuous O2/Ar ratio measurements by membrane inlet mass spectrometry, Geophys. Res. Lett., 32(19), 2005.
Keeling, R. F. and Shertz, S. R.: Seasonal and interannual variations in atmospheric oxygen and implications for the global carbon cycle, Nature, 358(6389), 723, 1992.
Kheireddine, M. and Antoine, D.: Diel variability of the beam attenuation and backscattering coefficients in the northwestern Mediterranean Sea (BOUSSOLE site), J. Geophys. Res. Ocean., 119(8), 5465–5482, 2014.
Kinkade, C. S., Marra, J., Dickey, T. D., Langdon, C., Sigurdson, D. E. and Weller, R.: Diel bio-optical variability observed from moored sensors in the Arabian Sea, Deep sea Res. Part II Top. Stud. Oceanogr., 46(8–9), 1813–1831, 1999.
Kostadinov, T. S., Siegel, D. A. and Maritorena, S.: Retrieval of the particle size distribution from satellite ocean color observations, J. Geophys. Res., 114(C9), C09015, doi:10.1029/2009JC005303, 2009.
Laws, E. A.: Photosynthetic quotients, new production and net community production in the open ocean, Deep Sea Res. Part A. Oceanogr. Res. Pap., 38(1), 143–167, 1991.
Lide, D. R.: Physical and optical properties of minerals, CRC Handb. Chem. Phys., 4–130, 1997.
Lochte, K., Ducklow, H. W., Fasham, M. J. R. and Stienen, C.: Plankton succession and carbon cycling at 47 N 20 W during the JGOFS North Atlantic Bloom Experiment, Deep Sea Res. Part II Top. Stud. Oceanogr., 40(1–2), 91–114, 1993.
Loisel, H., Nicolas, J.-M., Sciandra, A., Stramski, D. and Poteau, A.: Spectral dependency of optical backscattering by marine particles from satellite remote sensing of the global ocean, J. Geophys. Res., 111(C9), C09024, doi:10.1029/2005JC003367, 2006.
MacIntyre, H. L., Kana, T. M., Anning, T. and Geider, R. J.: Photoacclimation of irradiance response curves and photosynthetic pigments in microalgae and cyanobacteria, J. Phycol., 38(1), 17–38, doi:10.1046/j.1529-8817.2002.00094.x, 2002.
Manning, C. C., Stanley, R. H. R., Nicholson, D. P., Smith, J. M., Pennington, J. T., Fewings, M. R., Squibb, M. E. and Chavez, F. P.: Impact of recently upwelled water on productivity investigated using in situ and incubation-based methods in Monterey Bay, J. Geophys. Res. Ocean., 122(3), 1901–1926, 2017.

Marra, J.: Approaches to the measurement of plankton production, Phytoplankt. Product. Carbon Assim. Mar. Freshw. Ecosyst., 78–108, 2002.

Marra, J.: Net and gross productivity: weighing in with 14C, Aquat. Microb. Ecol., 56(2–3), 123–131, doi:10.3354/ame01306, 2009.

Morel, A., Huot, Y., Gentili, B., Werdell, P. J., Hooker, S. B. and Franz, B. A.: Examining the consistency of products derived from various ocean color sensors in open ocean (Case 1) waters in the perspective of a multi-sensor approach, Remote Sens. Environ., 111(1), 69–88, 2007.

Murphy, J. and Riley, J. P.: A modified single solution method for the determination of phosphate in natural waters, Anal. Chim. Acta, 27, 31–36, 1962.

Needham, D. M. and Fuhrman, J. A.: Pronounced daily succession of phytoplankton, archaea and bacteria following a spring bloom, Nat. Microbiol., 1(4), 16005, 2016.

Nicholson, D. P., Wilson, S. T., Doney, S. C. and Karl, D. M.: Quantifying subtropical North Pacific gyre mixed layer primary productivity from Seaglider observations of diel oxygen cycles, Geophys. Res. Lett., 42(10), 4032–4039, 2015.

Organelli, E., Bricaud, A., Antoine, D. and Matsuoka, A.: Seasonal dynamics of light absorption by chromophoric dissolved organic matter (CDOM) in the NW Mediterranean Sea (BOUSSOLE site), Deep Sea Res. Part I Oceanogr. Res. Pap., 91, 72–85, 2014.

Peacock, M., Evans, C. D., Fenner, N., Freeman, C., Gough, R., Jones, T. G. and Lebron, I.: UV-visible absorbance spectroscopy as a proxy for peatland dissolved organic carbon (DOC) quantity and quality: considerations on wavelength and absorbance degradation, Environ. Sci. Process. Impacts, 16(6), 1445–1461, 2014.

Raymond, P. A., Zappa, C. J., Butman, D., Bott, T. L., Potter, J., Mulholland, P., Laursen, A. E., McDowell, W. H. and Newbold, D.: Scaling the gas transfer velocity and hydraulic geometry in streams and small rivers, Limnol. Oceanogr. Fluids Environ., 2(1), 41–53, 2012.

Reuer, M. K., Barnett, B. A., Bender, M. L., Falkowski, P. G. and Hendricks, M. B.: New estimates of Southern Ocean biological production rates from O2/Ar ratios and the triple isotope composition of O2, Deep Sea Res. Part I Oceanogr. Res. Pap., 54(6), 951–974, 2007.

Ribalet, F., Swalwell, J., Clayton, S., Jiménez, V., Sudek, S., Lin, Y., Johnson, Z. I., Worden, A. Z. and Armbrust, E. V.: Light-driven synchrony of Prochlorococcus growth and mortality in the subtropical Pacific gyre, Proc. Natl. Acad. Sci., 112(26), 8008–8012, 2015.

Riley, J. P.: Grasshoff, K. [Ed.] 1976. Methods of seawater analysis. Verlag Chemie, Weinheim

and New York, xv+ 317 p. $43.60., 1977.
Roesler, C. S. and Barnard, A. H.: Optical proxy for phytoplankton biomass in the absence of photophysiology: Rethinking the absorption line height, Methods Oceanogr., 7, 79–94, 2013.
Savoye, N., Benitez-Nelson, C., Burd, A. B., Cochran, J. K., Charette, M., Buesseler, K. O., Jackson, G. A., Roy-Barman, M., Schmidt, S. and Elskens, M.: 234Th sorption and export models in the water column: a review, Mar. Chem., 100(3–4), 234–249, 2006.
Schuback, N., Flecken, M., Maldonado, M. T. and Tortell, P. D.: Diurnal variation in the coupling of photosynthetic electron transport and carbon fixation in iron-limited phytoplankton in the NE subarctic Pacific, Biogeosciences, 13, 1019–1035, doi:10.5194/bg-13-1019-2016, 2016.
Siegel, D. A., Dickey, T. D., Washburn, L., Hamilton, M. K. and Mitchell, B. G.: Optical determination of particulate abundance and production variations in the oligotrophic ocean, Deep Sea Res. Part A. Oceanogr. Res. Pap., 36(2), 211–222, 1989.
Stanley, R. H. R., Kirkpatrick, J. B., Cassar, N., Barnett, B. A. and Bender, M. L.: Net community production and gross primary production rates in the western equatorial Pacific, Global Biogeochem. Cycles, 24(4), 2010.
Stramska, M. and Dickey, T. D.: Short-term variations of the bio-optical properties of the ocean in response to cloud-induced irradiance fluctuations, J. Geophys. Res. Ocean., 97(C4), 5713–5721, 1992.
Stramska, M. and Dickey, T. D.: Modeling phytoplankton dynamics in the northeast Atlantic during the initiation of the spring bloom, J. Geophys. Res. Ocean., 99(C5), 10241–10253, 1994.
Stramska, M., Stramski, D., Hapter, R., Kaczmarek, S. and Ston´, J. S.: Bio-optical relationships and ocean color algorithms for the north polar region of the Atlantic, J. Geophys. Res, 108(C5), 3143, doi:10.1029/2001JC001195, 2003.
Stramski, D. and Kiefer, D. A.: Light scattering by microorganisms in the open ocean, Prog. Oceanogr., 28(4), 343–383, doi:10.1016/0079-6611(91)90032-H, 1991.
Stramski, D. and Reynolds, R. A.: Diel variations in the optical properties of a marine diatom, Limnol. Oceanogr., 38(7), 1347–1364, 1993.
Stukel, M. R., Aluwihare, L. I., Barbeau, K. A., Chekalyuk, A. M., Goericke, R., Miller, A. J., Ohman, M. D., Ruacho, A., Song, H. and Stephens, B. M.: Mesoscale ocean fronts enhance carbon export due to gravitational sinking and subduction, Proc. Natl. Acad. Sci., 114(6), 1252–

1257, 2017.
Sullivan, J. M., Twardowski, M. S., Donaghay, P. L. and Freeman, S. A.: Use of optical scattering to discriminate particle types in coastal waters, Appl. Opt., 44(9), 1667, doi:10.1364/AO.44.001667, 2005.
Thomas, A. C. and Weatherbee, R. A.: Satellite-measured temporal variability of the Columbia River plume, Remote Sens. Environ., 100(2), 167–178, doi:10.1016/J.RSE.2005.10.018, 2006.
Thomson, R. E., Fine, I. V., Thomson, R. E. and Fine, I. V.: Estimating Mixed Layer Depth from Oceanic Profile Data, J. Atmos. Ocean. Technol., 20(2), 319–329, doi:10.1175/1520-0426(2003)020<0319:EMLDFO>2.0.CO;2, 2003.
Thyssen, M., Grégori, G. J., Grisoni, J.-M., Pedrotti, M. L., Mousseau, L., Artigas, L. F., Marro, S., Garcia, N., Passafiume, O. and Denis, M. J.: Onset of the spring bloom in the northwestern Mediterranean Sea: influence of environmental pulse events on the in situ hourly-scale dynamics of the phytoplankton community structure, Front. Microbiol., 5, 387, 2014.
Tortell, P. D.: Dissolved gas measurements in oceanic waters made by membrane inlet mass spectrometry, Limnol. Oceanogr. Methods, 3(1), 24–37, 2005.
Tortell, P. D., Guéguen, C., Long, M. C., Payne, C. D., Lee, P. and DiTullio, G. R.: Spatial variability and temporal dynamics of surface water pCO2, ΔO2/Ar and dimethylsulfide in the Ross Sea, Antarctica, Deep Sea Res. Part I Oceanogr. Res. Pap., 58(3), 241–259, 2011.
Tortell, P. D., Asher, E. C., Ducklow, H. W., Goldman, J. A. L., Dacey, J. W. H., Grzymski, J. J., Young, J. N., Kranz, S. A., Bernard, K. S. and Morel, F. M. M.: Metabolic balance of coastal Antarctic waters revealed by autonomous pCO2 and ΔO2/Ar measurements, Geophys. Res. Lett., 41(19), 6803–6810, 2014.
Turner, R. E., Qureshi, N., Rabalais, N. N., Dortch, Q., Justic, D., Shaw, R. F. and Cope, J.: Fluctuating silicate: nitrate ratios and coastal plankton food webs, Proc. Natl. Acad. Sci., 95(22), 13048–13051, 1998.
Twardowski, M. S., Boss, E., Macdonald, J. B., Pegau, W. S., Barnard, A. H. and Zaneveld, J. R. V.: A model for estimating bulk refractive index from the optical backscattering ratio and the implications for understanding particle composition in case I and case II waters, J. Geophys. Res. Ocean., 106(C7), 14129–14142, doi:10.1029/2000JC000404, 2001.
Wanninkhof, R.: Relationship between wind speed and gas exchange over the ocean revisited, Limnol. Oceanogr. Methods, 12(6), 351–362, 2014.

Weiss, R. F. and Price, B. A.: Nitrous oxide solubility in water and seawater, Mar. Chem., 8(4), 347–359, 1980.

Westberry, T., Behrenfeld, M. J., Siegel, D. A. and Boss, E.: Carbon-based primary productivity modeling with vertically resolved photoacclimation, Global Biogeochem. Cycles, 22(2), 2008.

White, A. E., Barone, B., Letelier, R. M. and Karl, D. M.: Productivity diagnosed from the diel cycle of particulate carbon in the North Pacific Subtropical Gyre, Geophys. Res. Lett., 44(8), 3752–3760, 2017.

Whitney, F. . and Freeland, H. .: Variability in upper-ocean water properties in the NE Pacific Ocean, Deep Sea Res. Part II Top. Stud. Oceanogr., 46(11–12), 2351–2370, doi:10.1016/S0967-0645(99)00067-3, 1999.

Wu, C.-J., Chiang, K.-P. and Liu, H.: Diel feeding pattern and prey selection of mesozooplankton on microplankton community, J. Exp. Mar. Bio. Ecol., 390(2), 134–142, 2010.

Zeng, C., Rosengard, S. Z., Burt, W., Peña, M. A., Nemcek, N., Zeng, T., Arrigo, K. R. and Tortell, P. D.: Optically-derived estimates of phytoplankton size class and taxonomic group biomass in the Eastern Subarctic Pacific Ocean, Deep Sea Res. Part I Oceanogr. Res. Pap., 136, 107–118, 2018.

Table 1: Daily-integrated mixed layer net primary production (NPP) and net community production (NCP), including all components used to calculate NCP using $\Delta O_2/Ar$ or POC time series, as indicated: gross primary productivity (GPP), respiration (R), vertical mixing (Mix), and gas exchange (J_{ex}). Daily integrated NCP calculated over 3 hour intervals are also listed for comparison. Derived POC export estimates assuming 40% and 28% $DOC/NCP_{O2/Ar}$ during drifter periods 1 and 2, respectively, are provided, as well. All units here are in mmol C m^{-2} d^{-1}. Note that CbPM is the carbon-based production model (Sect. 2.5).

	Drifter 1:			**Drifter 2:**	
	Day 1	**Day 2**	**Day 3**	**Day 1**	**Day 2**
NPP (CbPM)	147 ± 61	137 ± 51	112 ± 40	22 ± 9	18 ± 7
NPP (^{14}C)	150 ± 18	-	49 ± 8	12 ± 4	-
GPP ($\Delta O_2/Ar$)	289 ± 51	267 ± 33	356 ± 44	108 ± 28	219 ± 47
GPP (POC)	211 ± 47	130 ± 47	115 ± 53	41 ± 8	38 ± 7
R ($\Delta O_2/Ar$)	-68 ± 67	-154 ± 37	-173 ± 39	-83 ± 36	-186 ± 65
R (POC)	-108 ± 51	-123 ± 48	-87 ± 56	-44 ± 12	-36 ± 9
Mix (N_2O)	75 ± 28	12 ± 8	17 ± 9	0	0
Mix (POC)	36 ± 43	36 ± 43	36 ± 43	0	0
J_{ex} (daily)	-62 ± 11	-7 ± 4	-6 ± 3	16 ± 5	21 ± 7
$NCP_{O2/Ar}$	146 ± 43	100 ± 28	166 ± 40	26 ± 18	33 ± 20
NCP_{POC}	66 ± 45	-29 ± 47	-9 ± 51	-3 ± 3	1 ± 2
$NCP_{O2/Ar}$ (3 hr)	183	126	120	-12	25
NCP_{POC} (3 hr)	87	-63	69	-8	-6
POC export	21	89	108	21	23

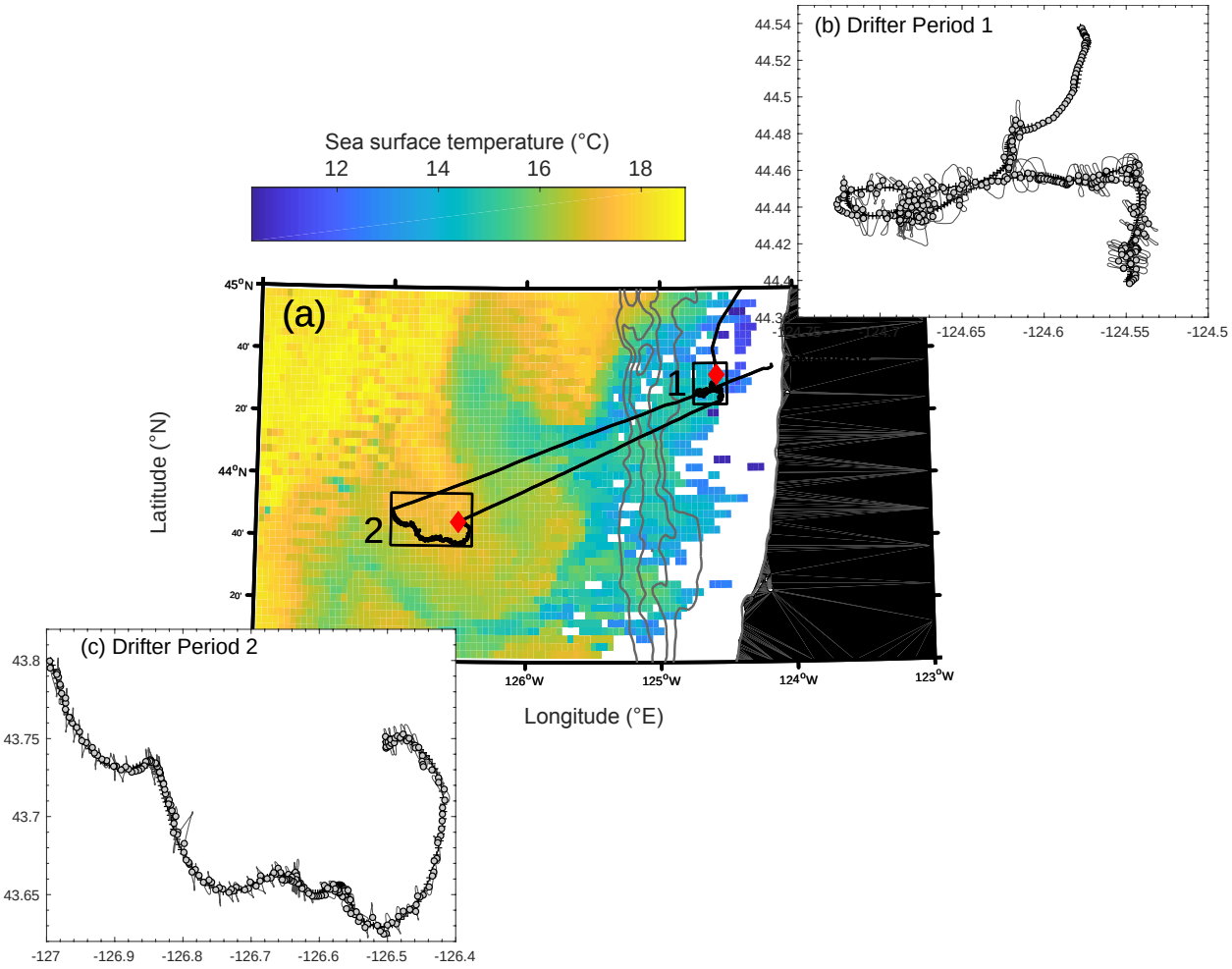

Figure 1: (a) Map of AQUA MODIS-derived 8-day composite sea surface temperature (11µm, nighttime) from 21-28 August 2017, overlapping with the duration of both drifter deployments. The two hollow boxes on the map denote location of drifter tracks, with the red diamonds indicating the location of the initial release. Gray bathymetry contours extend from 0-2000 m, with deepest contours representing the extent of the continental shelf. Panels (b and c) show a detailed view of the two drifter tracks, with the ship's track shown in a light grey line and circles denoting times when the ship was <1.5 km away from the drifter position. Only measurements taken at these cross-over locations were used for analysis.

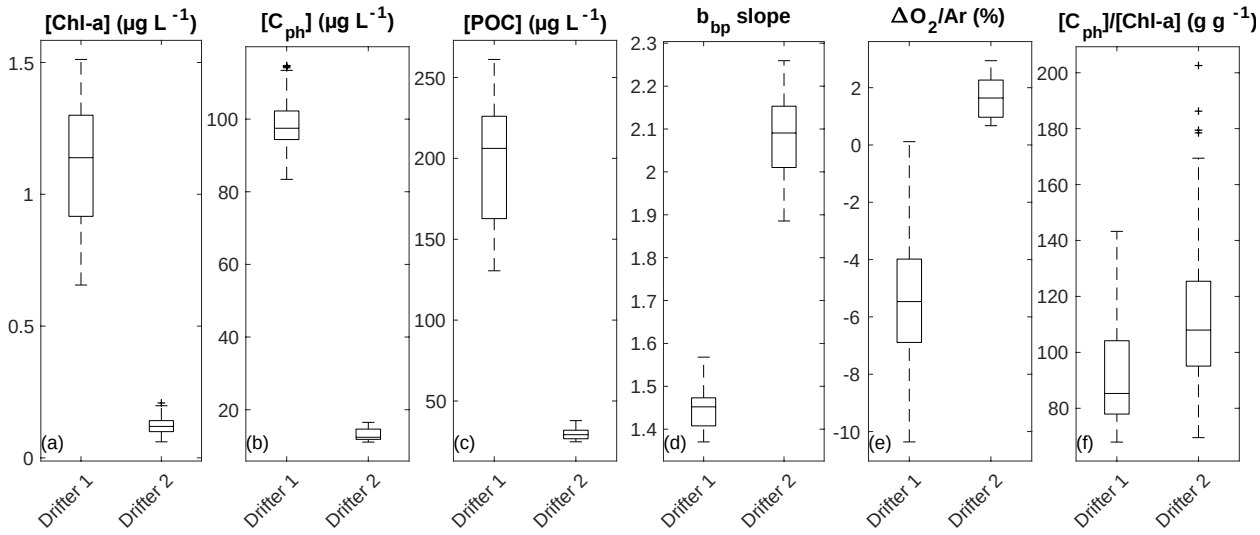

Figure 2: Comparison of average surface water properties between the two drifter deployments: (a) chlorophyll-a concentration (Chl-a), (b) phytoplankton carbon concentration (C_{ph}), (c) particulate organic carbon (POC) concentration, (d) the wavelength-dependent slope of particulate backscatter (b_{bp}), (e) biological oxygen saturation anomaly ($\Delta O_2/Ar$), and (f) the $[C_{ph}]/[Chl\text{-}a]$ ratio. Boxes represent the median (center line) and 25 and 75 percentiles (box edges). Outliers are indicated as black "+" marks.

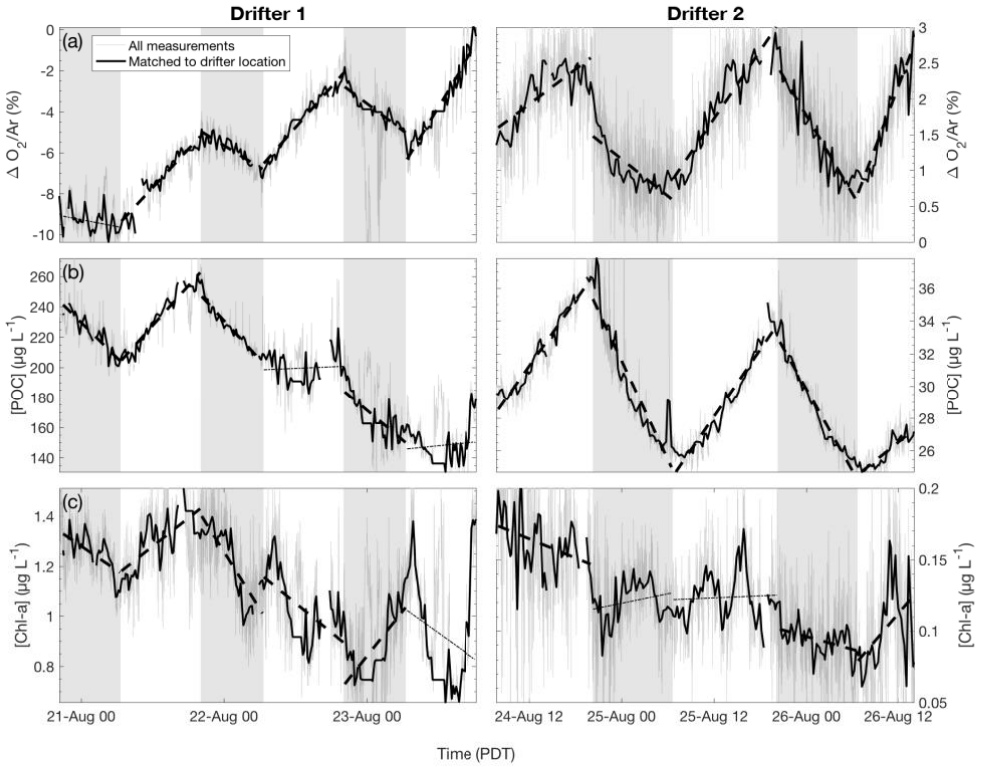

Figure 3: Time-series of (a) biological oxygen saturation ($\Delta O_2/Ar$), (b) particulate organic carbon (POC) concentration, and (c) chlorophyll-a (Chl-a) concentration during the two drifter deployments (left and right panels, respectively). For each daytime (non-shaded) and nighttime (shaded) interval, the best fit linear regression line is plotted. Significant regressions ($p<0.05$) are plotted as thick dashed lines, while non-significant regressions ($p\geq0.05$) are plotted as thin dotted lines. Grey lines show all measurements while thicker black line shows observations collected when the ship was within 1.5 km of the drifter location.

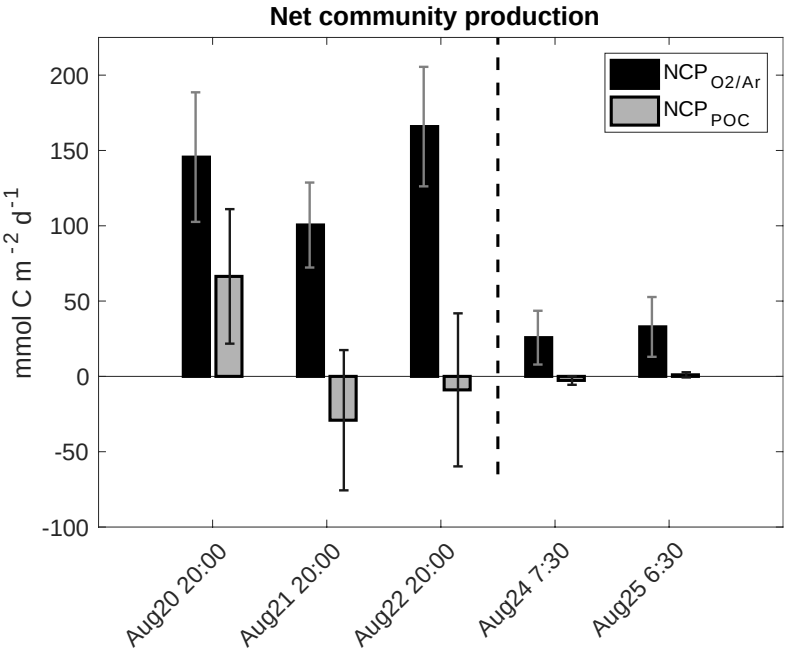

Figure 4: Daily net community production (NCP) during successive days of the two drifter deployments derived from diurnal variations of biological oxygen saturation ($\Delta O_2/Ar$), and particulate organic carbon (POC) concentration. Each set of bars is for one 24-hour period, with approximate starting times on the x-axis.